Traction force microscopy for linear and nonlinear elastic materials as a parameter identification inverse problem

OPEN ACCESS
IOP Publishing
Inverse Problems

Inverse Problems **41** (2025) 065023 (30pp) https://doi.org/10.1088/1361-6420/add0d5

Traction force microscopy for linear and nonlinear elastic materials as a parameter identification inverse problem

Gesa Sarnighausen[1], Tram Thi Ngoc Nguyen[2], Thorsten Hohage[1], Mangalika Sinha[3,5], Sarah Köster[3,5], Timo Betz[4,5], Ulrich Sebastian Schwarz[6,7] and Anne Wald[1,*]

[1] Institute for Numerical and Applied Mathematics, University of Göttingen, Göttingen, Germany
[2] Max Planck Institute for Solar System Research, Göttingen, Germany
[3] Institute for X-Ray Physics, University of Göttingen, Göttingen, Germany
[4] Third Institute of Physics, Biophysics/ Complex Systems, University of Göttingen, Göttingen, Germany
[5] Cluster of Excellence "Multiscale Bioimaging: From Molecular Machines to Networks of Excitable Cells" (MBExC), University of Göttingen, Göttingen, Germany
[6] Institute for Theoretical Physics, Heidelberg University, Heidelberg, Germany
[7] BioQuant, Heidelberg University, Heidelberg, Germany

E-mail: a.wald@math.uni-goettingen.de, g.sarnighausen@math.uni-goettingen.de, nguyen@mps.mpg.de, hohage@math.uni-goettingen.de, mangalika.sinha@uni-goettingen.de, timo.betz@phys.uni-goettingen.de, schwarz@thphys.uni-heidelberg.de and sarah.koester@uni-goettingen.de

Received 29 November 2024; revised 28 March 2025
Accepted for publication 25 April 2025
Published 19 June 2025

Abstract

Traction force microscopy (TFM) is a method widely used in biophysics and cell biology to determine forces that biological cells apply to their environment. In the experiment, the cells adhere to a soft elastic substrate, which is then deformed in response to cellular traction forces. The inverse problem consists

* Author to whom any correspondence should be addressed.

in computing the traction stress applied by the cell from microscopy measurements of the substrate deformations. In this work, we consider a linear model, in which 3D forces are applied at a 2D interface, called 2.5D TFM, and a nonlinear pure 2D model, from which we directly obtain a linear pure 2D model. All models lead to a linear resp. nonlinear parameter identification problem for a boundary value problem of elasticity. We analyze the respective forward operators and conclude with some numerical experiments for simulated and experimental data.

Keywords: inverse problems, parameter identification, elasticity, traction force microscopy, regularization

1. Introduction

Cells are the fundamental building blocks of all living systems. They consist of a multitude of biomolecules that continuously interact with each other and thereby form distinct structures. In particular, a large number of proteins are involved in building the cytoskeleton, which is a system of different types of filaments that together give mechanical stability to cells, which they need to move, divide and form tissue [38]. Biological systems are active in the sense that they continuously consume energy and thus keep the system away from thermodynamic equilibrium. This not only allows them to form structures that are not possible in equilibrium, it also allows them to quickly adapt to changes in their environment [2, 6]. A particular point in case are molecular motors, which are large proteins that use energy to undergo conformational changes that lead to force generation. Together with other force-generating processes like polymerization, this activity allows cells to change their shape, migrate, divide, and adhere to surfaces and other cells. Because it is difficult to measure cell forces inside cells, it has become a standard procedure in biophysics and cell biology to measure them at the interface between the cells and their environment, with a procedure called traction force microscopy (TFM) [19, 36, 53, 60, 69].

In TFM, cells are cultured on soft elastic substrates. Fiducial markers, i.e. small fluorescent beads, are embedded in the substrate and the displacement of the substrate is calculated by comparing observed images of the markers first with and again without applied traction stresses (compare figure 1). This imaging task of computing the displacement is of course an interesting problem and can be solved in many different ways, e.g. using optical flow [12, 39], but is not within the scope of this work. The inverse problem then consists in computing the traction stresses given the displacement, which are related via the boundary value problem (BVP) of elasticity for the substrate. Depending on the chosen material law the BVP can be linear or nonlinear. Hence, we refer to linear or nonlinear TFM.

When cells are plated on a planar substrate coated with proteins from the extracellular matrix (ECM), they spread out to increase surface contact with the substrate and to establish stable adhesions. Thus, they tend to thin out, as a result of which the cellular forces are predominantly in-plane. This effect is further enhanced by the fact that for adhesion to a planar substrate, the cytoskeleton typically flows parallel to the substrate, from the periphery to the center, thus also generating mainly tangential (and centrally directed) forces. This explains the name ‘traction force’, i.e. the force acting tangentially on the substrate plane, similar to a car on the road. However, in general, cellular traction forces need not be tangential, because several aspects are leading also to forces in the perpendicular direction, including the large nucleus sticking out into the third dimension, cortical tension pulling everywhere in the cell envelope, and the internal organization of the adhesion sites [19, 60]. For example, cancer cells often try to invade

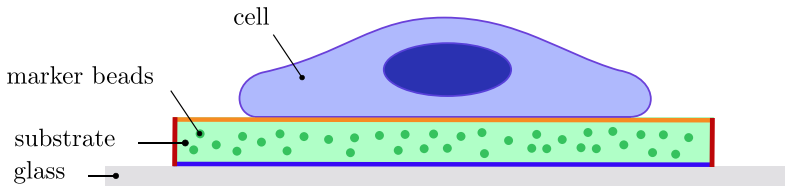

(a) Experimental setup for TFM.

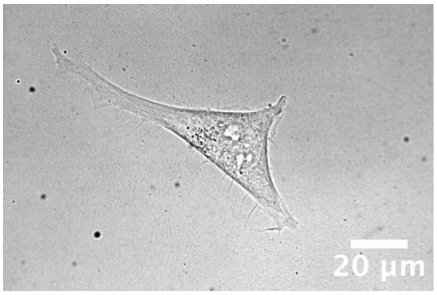

(b) Microscopy image of a cell.

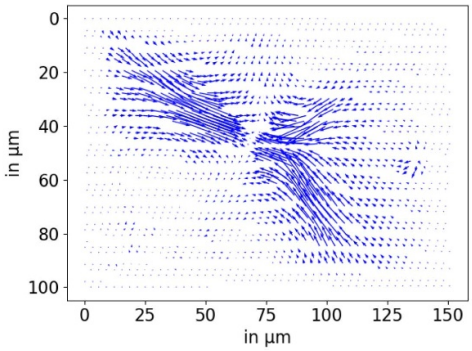

(c) Image of the deformation.

Figure 1. (a) Experimental setup for TFM. Small fiducial markers (dark green) are embedded in a soft elastic substrate (light green). The cell (blue; nucleus in dark blue) adheres to the substrate and applies traction stresses. For 2D TFM one often only uses and follows markers in a thin layer just underneath the substrate surface, as only tangential deformations are being considered. For 2.5D TFM the markers have to be followed in three dimensions, because one also has to track perpendicular deformations. In practice, the substrate is much thicker than the force generating structures in the cell (about 50 μm vs a few μm). The markers are typically imaged with an inverse optical microscope from below. (b) Microscopy image of a cell plated on a planar substrate. (c) Image of the corresponding deformation.

the substrate, and then sometimes use their nucleus to generate perpendicular forces onto the substrate [34].

The output of TFM typically is a map of traction stress measured in physical units of $\mathrm{Pa} = \mathrm{N\,m^{-2}}$. A typical value for cellular traction forces is kPa, which makes sense because this is also the typical value of the stiffness of an ECM. Only if these two numbers are of similar magnitude, the cell and its environment are at a reasonable mechanical balance to each other [51]. Although from the viewpoint of elasticity theory, one measures stress and not force, this technique is called TFM because the whole notion of this technique lies in understanding the forces exerted by the cells on the substrate.

One of the most exciting aspects of cell mechanics research is to establish a connection between cellular level force generation and the underlying molecular mechanisms. TFM serves as a crucial tool in the field of cell mechanics providing valuable insights into how cells interact with their environment. TFM enables the quantitative measurement of forces exerted by cells on their surroundings, which is essential for understanding various biological processes like cell migration, adhesion and division.

Traction force observations were first developed in 1980 by Harris *et al* who were the first to culture cells on a substrate and observe the traction stresses of the cells by wrinkling and

elastic distortion of the substrate [25, 26]. Over 10 years later Dembo *et al* developed the first TFM method by finding a way to quantitatively compute the applied stresses from the measured displacement, first for thin films [17] and then for thick ones [18]. For thick films, they considered a linear 2D model, ignoring the normal component, and then used Green's functions from the analytical Boussinesq solution for the elastic halfspace, i.e. they assume an infinite substrate with homogeneous Dirichlet boundary conditions at infinity, leading to an ill-posed inverse problem, and solved it in real space. It is also possible to solve the inverse problem in Fourier space without regularization [15]. Since the inverse problem is ill-posed, noisy data can lead to severe artifacts in the reconstruction if no regularization is used [52]. Therefore, regularization was also incorporated into the Fourier space setting [46, 47]. This method is now mostly used in practice to reconstruct traction stresses and in the following we will refer to this approach as the 'standard' approach. A specific numerical realization of this is called 'Fourier Transform Traction Cytometry', in short 'FTTC' [10]. Note, that even if this approach is called 2D TFM, due to the use of the Boussinesq solution the model is not purely 2D.

If the substrate cannot be modeled by a linear material law, the standard approach does not work anymore since there exists no analytical Boussinesq solution for the underlying BVP. In this case, finite element methods can be used, e.g. by solving a PDE-constrained optimization problem as in Ambrosi *et al* [3, 4]. Michel *et al* have proposed a mathematical framework both for Ambrosi's solution approach and the standard Fourier method [41]. It is further possible to solve the BVP of elasticity with respect to the stress σ and then directly compute the traction stresses t by the relationship $t = \sigma n$, where n is the normal vector [32, 33].

TFM can also be formulated as a direct problem, by calculating stress directly from strain [7, 10, 21, 40]. However, high-quality and three-dimensional measurements are necessary because the direct method includes taking derivatives of the noisy measured data. This approach is often used in 2.5D and 3D due to the lack of an analytical solution for the respective BVP.

Another strategy is model-based TFM, when traction forces are not reconstructed at the substrate surface, but directly fitted against a physical model of force generation. While this makes the results depend on the chosen model, it allows us to gain information about how the traction stresses are distributed in the cell by incorporating modeling assumptions on the cells [44, 57, 62, 63]. Similar to direct TFM, high quality measurements are necessary to obtain reasonable results.

During the last three decades since its invention, TFM has matured into a large research area, and many different experimental setups and solution strategies have been devised. To systematize the field, it is helpful to make a few distinctions. One important distinction is between direct and inverse approaches; while in the direct method stresses are directly calculated from strains, in the inverse method, stresses are estimated as minimizers of the differences between predicted and observed displacements [10]. Another helpful distinction can be made between 2D, 2.5D, compare figure 1, and 3D TFM [53]. The 2D setting is the simplest. A cell is placed onto a planar soft elastic substrate with marker beads and one follows their deformations. By ignoring the normal component of cell forces and displacement, it is assumed that the cell forces are just two-dimensional. 3D TFM refers to a cell completely embedded inside a 3D matrix, e.g. hydrogel gel, with beads all around it. In principle, it is then possible to determine three-dimensional traction forces around the whole cell. However, the imaging of the displacement is very difficult and time-consuming in 3D. More importantly, the material law for 3D material allowing for 3D TFM is typically very complex [58, 59] and often not even elastic [66]. Therefore, a good compromise is 2.5D TFM. As in 2D TFM, a cell is placed on a planar substrate as shown in figure 1. However, marker beads are not only tracked in a plane, but in all three dimensions. In this article, we will consider both pure 2D and 2.5D TFM.

Even though TFM is widely used in biophysics and cell biology, the mathematical literature on TFM is scarce [3, 41]. This article aims to develop a rigorous mathematical theory in a function space setting for both linear and nonlinear TFM and to solve the inverse problem efficiently by regularization methods. We analyze a continuous model and only discretize for implementation, while previous approaches often discretize already the initial model. In linear/nonlinear TFM a linear/nonlinear material as a substrate and the corresponding linear/nonlinear strain tensor are used leading to a linear/nonlinear inverse problem, respectively. Most materials are linear at small deformations, which can be ensured by using a material that is a bit stiffer than typical traction forces. However, stiff materials typically change cell behavior, and thus one often also uses soft materials and large deformations, which might require nonlinear material laws.

We first solve the linear inverse problem of 2.5D TFM with a three-dimensional substrate using a similar method as Soiné *et al* [56]. With our functional analytic setting, we can easily apply different standard algorithms from the theory of inverse problems. We then solve the nonlinear inverse problem in a pure 2D setting for the substrate's surface and a hyperelastic material law. Hyperelasticity is a mathematical concept as introduced in section 2.1. One method used by a number of groups for solving nonlinear TFM is the direct method [8, 10, 21], i.e. directly computing traction forces from the measured data by numerically differentiating the noisy data. As in the linear 2.5D case, we propose a model formulation that can be solved in a straightforward manner using different regularization methods. From this approach, we directly derive a solution method for linear pure 2D TFM which is used for experimental data in section 4.4. We can use this approach either for computing the traction if the effective thickness is known or for estimating the effective thickness beyond which the horizontal displacements disappear. As described above, this approach differs from the standard approach because the use of the Boussinesq solution makes the model not purely 2D, whereas we consider a pure 2D model.

In summary, this article provides a rigorous mathematical analysis for linear and nonlinear pure 2D TFM as well as 2.5D linear TFM along with all necessary tools to solve these inverse problems numerically in a stable way. It can be seen as a mathematical basis to allow for nonlinear substrate materials. Real biological materials are in most cases nonlinear. Polyacrylamide (PAA) which is commonly used in linear TFM is not and one would not deliberately do an experiment with a more complicated, nonlinear material; but if a biological material is used, e.g. protein networks, one has to deal with the nonlinearity.

Outline. In this article, we propose a TFM model leading to a parameter identification problem that can be solved using functional analytic tools and regularization methods from inverse problems theory. We propose a linear 2.5D model and a nonlinear pure 2D model which automatically leads to an analogous linear pure 2D model as well. The article is structured as follows. The first part deals with the linear 2.5D model, see section 2. After presenting the basics of elasticity theory in section 2.1, the linear mathematical model is derived and analyzed in section 2.2. In the second part (section 3), we first derive the nonlinear model in section 3.1. Then the well-posedness of the forward operator is investigated, see section 3.2, and the Fréchet derivative and its adjoint are computed in section 3.4. The third part, section 4, contains various numerical experiments for both simulated and experimentally measured data.

2. Linear 2.5D TFM

If the substrate is modeled by a linear material law, the traction stress t and the displacement u are connected by the linear displacement-traction BVP of elasticity. With a forward operator

that maps a traction stress t to the corresponding displacement u, we can consider TFM as a linear parameter identification problem.

2.1. Basics of elasticity

Let $n \in \{2,3\}$. For a deformation $\varphi : \mathbb{R}^n \to \mathbb{R}^n$, we define the displacement vector $u(x) := \varphi(x) - x$. Using this definition, we can express the deformation gradient $F := \nabla\varphi(x) \in \mathbb{R}^{n\times n}$ as

$$F(t,x) = \nabla u(x) + I \in \mathbb{R}^{n\times n}, \tag{1}$$

where I is the identity matrix. The deformation gradient is used to define a nonlinear strain tensor, the Green–Lagrange tensor

$$E := \frac{1}{2}\left(F^\top F - I\right) \in \mathbb{R}^{n\times n}. \tag{2}$$

The Green–Lagrange tensor E is often represented as

$$E = \frac{1}{2}\left(\nabla u + (\nabla u)^\top + (\nabla u)^\top (\nabla u)\right) \in \mathbb{R}^{n\times n} \tag{3}$$

by means of (1). For small strains ε resp. deformations, one often uses the linearized Green–Lagrange tensor

$$\varepsilon := \frac{1}{2}\left(\nabla u + (\nabla u)^\top\right) \in \mathbb{R}^{n\times n}, \tag{4}$$

omitting the high-order term. These basic equations of elasticity can be found e.g. in [16, chapter 1.8]. The relation between the strain tensor ε or E and the first Piola–Kirchhoff stress tensor σ on the undeformed region is called a constitutive equation and depends on the material. For simplicity we will refer to σ only as the stress tensor.

Remark 2.1 (Lagrangian vs Eulerian descriptions). Throughout this paper we use a Lagrangian description, i.e. physical quantities are represented by functions defined on the undeformed region and a given argument corresponds to a fixed point of the material. In contrast, a Eulerian description, useful for many physical considerations, represents physical quantities by functions defined on the deformed region such that a given argument corresponds to a fixed point in space.

If the substrate material is linear elastic and isotropic, we have a linear constitutive relation between ε and σ, given by Hooke's law (see, e.g. [16, chapter 6.2])

$$\sigma(u) = \lambda \operatorname{div}(u) I + 2\mu\varepsilon \in \mathbb{R}^{n\times n} \tag{5}$$

in terms of the Lamé constants $\lambda, \mu \in \mathbb{R}$, related to the Young modulus $\tilde{E}$ and the Poisson ratio ν via

$$\mu = \frac{\tilde{E}}{2(1+\nu)} > 0, \quad \lambda = \frac{\tilde{E}\nu}{(1+\nu)(1-2\nu)}, \tag{6}$$

see [16, chapter 3.8]. The first Lamé parameter λ is positive for a positive Poisson ratio $\nu < \frac{1}{2}$. Here, we only consider this case.

Figure 2. Substrate Ω with boundary $\partial\Omega = \Gamma_T \cup \Gamma_{T_0} \cup \Gamma_D$ and outer normal vectors n.

A material is called hyperelastic if there exists a function $W(F)$, called the stored energy function, such that

$$\sigma(x,F) = \frac{\partial W}{\partial F}(x,F), \tag{7}$$

see, e.g. [70, chapter 61.6] or [16, chapter 4]). Hyperelastic constitutive equations model non-linear material behavior as well as large shape changes. Examples of constitutive equations and their physical background can be found in [13, chapter 3.5] or, with a stronger emphasis on mathematics, in [11]. More details about elasticity and all the above equations can be found, e.g. in [16, 30] or [70, chapter 61/62].

2.2. A mathematical model of linear 2.5D TFM

Consider a non-deformed region $\emptyset \neq \Omega \subset \mathbb{R}^3$ which is bounded, open and connected with a smooth boundary $\partial\Omega \in C^{0,1}$ and $\partial\Omega = \overline{\Gamma_D} \cup \overline{\Gamma_{T^*}}$ for disjoint, relatively open subsets $\Gamma_D, \Gamma_{T^*} \subset \partial\Omega$ and $\Gamma_D \neq \emptyset$. In the case of TFM the region of interest is part of the substrate which is assumed to be a cuboid, see figures 1 and 2. The bottom surface of the cuboid is called Γ_D, the side surface Γ_{T_0} and the top surface Γ_T with $\Gamma_{T^*} = \Gamma_T \cup \Gamma_{T_0}$.

The balance of internal and body forces is expressed as $-\operatorname{div}\sigma = f$ in Ω where the forces f acting on the whole substrate, e.g. gravity, are neglected in the context of TFM. Therefore, we assume in the following $f = 0$.

The traction stresses that the cell exerts onto the substrate can be modeled as surface forces acting on the boundary of the substrate by $\sigma n = t$ on Γ_{T_*} where n is the outer normal vector, see figure 2. Since the cell applies forces only to the upper surface Γ_T, we have $t = 0$ on the side surface Γ_{T_0}. Therefore, we will consider the traction stress t only as a function on the upper surface Γ_T in the following. Furthermore, the displacement on the lower surface Γ_D is zero because the substrate is fixed to the glass. Altogether, given traction stresses $t \in L^2(\Gamma_T, \mathbb{R}^3)$ we obtain the mixed BVP of elasticity:

$$\begin{cases} -\operatorname{div}\sigma(u) = 0 & \text{in } \Omega \\ \sigma(u)n = t & \text{on } \Gamma_T \\ \sigma(u)n = 0 & \text{on } \Gamma_{T_0} \\ u = 0 & \text{on } \Gamma_D, \end{cases} \tag{8}$$

where $\sigma(u)$ is given by Hooke's law (5). Next we derive a weak formulation in the space

$$H^1_{0,\Gamma_D}(\Omega,\mathbb{R}^3) := \left\{u \in H^1(\Omega,\mathbb{R}^3) : u|_{\Gamma_D} = 0\right\} \quad \text{with} \quad \|v\|_{H^1_{0,\Gamma_D}(\Omega,\mathbb{R}^3)} := \|\nabla v\|_{L^2(\Omega,\mathbb{R}^3)}.$$

It follows from Tartar's equivalence lemma [64] that $\|\cdot\|_{H^1_{0,\Gamma_D}}$ is a Hilbert norm equivalent to the standard H^1-norm.

The weak formulation of problem (8) is given by

$$\text{find } u \in H^1_{0,\Gamma_D}\left(\Omega,\mathbb{R}^3\right) \quad \text{s.t.} \quad a(u,v) = l_t(v) \text{ for all } v \in H^1_{0,\Gamma_D}\left(\Omega,\mathbb{R}^3\right) \tag{9}$$

with the bilinear form a and the linear form l_t defined by

$$a(u,v) := \int_\Omega 2\mu\varepsilon(u) : \varepsilon(v) + \lambda \operatorname{div}(u)\operatorname{div}(v)\,\mathrm{d}x, \quad l_t(v) := \int_{\Gamma_T} tv\,\mathrm{d}s.$$

Here $(M:M) := |M|_{\mathrm{F}}^2 = \sum_{i,j=1}^n M_{ij}^2$ for matrices $M \in \mathbb{R}^{n\times n}$ is the Frobenius inner product with corresponding Frobenius norm $|\cdot|_{\mathrm{F}}$.

It follows from a standard application of the Lax–Milgram lemma and Korn's inequality that the parameter-to-state-map of linear TFM

$$A : L^2\left(\Gamma_T,\mathbb{R}^3\right) \to H^1_{0,\Gamma_D}\left(\Omega,\mathbb{R}^3\right), \quad t \mapsto u, \tag{10}$$

which is defined by (9), is well-posed, linear, and bounded. The inverse problem consists in recovering the traction stresses t from a given displacement u.

Remark 2.2. The forward operator of linear TFM is given by the composition of the embedding to L^2 and parameter-to-state-map since we can only measure the L^2-error and norm of the measured displacement. All in all we get a forward operator

$$\hat{A} : L^2\left(\Gamma_T,\mathbb{R}^3\right) \to H^1_{0,\Gamma_D}\left(\Omega,\mathbb{R}^3\right) \hookrightarrow L^2\left(\Omega,\mathbb{R}^3\right), \quad t \mapsto u.$$

We need to compute the adjoint operator to use regularization algorithms, e.g. in the normal equations, see equation (34).

Lemma 2.3. *The adjoint operator* $\hat{A}^* : L^2(\Omega,\mathbb{R}^3) \to L^2(\Gamma_T,\mathbb{R}^3)$ *is given by*

$$\hat{A}^* w = \operatorname{tr}\phi$$

where the function ϕ *solves*

$$a(\phi,v) = \langle w,v\rangle_{L^2(\Omega,\mathbb{R}^3)} \quad \forall v \in H^1_{0,\Gamma_D}\left(\Omega,\mathbb{R}^3\right) \tag{11}$$

and $\operatorname{tr}\phi$ *denotes its trace on* Γ_T.

Proof. Let a traction stress $t \in L^2(\Gamma_T,\mathbb{R}^3)$ be arbitrary and define $u := \hat{A}t$. Then we obtain

$$\begin{aligned}\langle \hat{A}t, w\rangle_{L^2(\Omega,\mathbb{R}^3)} &= \langle u,w\rangle_{L^2(\Omega,\mathbb{R}^3)} = a(\phi,u) = a(u,\phi)\\ &= \langle t, \operatorname{tr}\phi\rangle_{L^2(\Gamma_T,\mathbb{R}^3)} = \langle t,\hat{A}^* w\rangle_{L^2(\Gamma_T,\mathbb{R}^3)}.\end{aligned}$$

It remains to show that (11) has a unique solution, which can be done again by Lax–Milgram since the bilinear form a is continuous and coercive and the linear form $l_w^*(v) := \langle w,v\rangle_{L^2(\Omega,\mathbb{R}^3)}$ is continuous. □

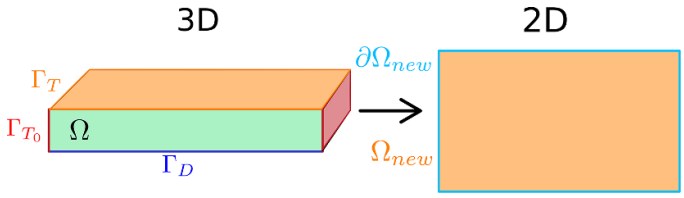

Figure 3. Change of TFM setting from 3D to 2D substrate.

3. Nonlinear pure 2D TFM

The linear model works well for small strains and linear materials. If we have larger strains we cannot assume anymore that the nonlinear part $(\nabla u)^\top \nabla u$ in (3) is small and neglect it. Therefore, we use the Green–Lagrange strain tensor (2) instead of the linearized strain tensor. Furthermore, if a nonlinear material is used, we need to find a suitable constitutive equation as a material law that describes the stress $\sigma(u)$.

These changes lead to a nonlinear PDE and thus to a nonlinear inverse problem.

3.1. Mathematical 2D model and inverse problem for a nonlinear material

In the nonlinear case, we consider a pure two-dimensional model, i.e. we only describe the surface of the substrate to which the cell adheres (see figure 3). For a deformation $\varphi : \mathbb{R}^2 \to \mathbb{R}^2$, we define, as before in section 2.1, the displacement vector $u(x) = \varphi(x) - x$, the Green–Lagrange strain tensor $E = \frac{1}{2}\left(\nabla u + (\nabla u)^\top + (\nabla u)^\top \nabla u\right)$ and the stress tensor $\sigma(u)$ given by a suitable material law to be specified later in section 3.3.

If the undeformed region can be modeled by a bounded, open, and connected domain $\Omega \subset \mathbb{R}^2$ with a Lipschitz continuous boundary $\partial\Omega$, the problem of TFM can be described by the BVP

$$\begin{cases} -\operatorname{div}(\sigma(u)) = T := \frac{t}{h} & \text{in } \Omega \\ u = 0 & \text{on } \partial\Omega \end{cases} \tag{12}$$

for traction stresses t with zero boundary conditions, effective thickness h, and the force density T. The effective thickness h is the thickness beyond which the horizontal displacements disappear [41]. The stress σ as described in (7) is the derivative of the material-dependent stored energy $W(F)$, the focus of the upcoming sections. The first equation in (12) is called the thickness-averaged condition for stress equilibrium [17, 35, 41]. We can use this approach either for computing the quantitative traction if the effective thickness is known or for estimating the effective thickness. Without knowing the effective thickness, we still get a qualitative result for the traction since h is only a multiplicative factor.

In the linear case, we considered the mixed BVP of elasticity with traction and displacement boundary conditions in 3D. If we change the model to the two-dimensional case, we neglect that the substrate is three-dimensional and only consider the upper surface of the substrate as our domain with the thickness-averaged condition for stress equilibrium [17]. This model has been used in, e.g. [17, 41]. However the standard model assumes an infinitely large halfspace leading to a model that is not purely nonlinear, see, e.g. [18, 53].

By consequence, in the 2D case here, the old upper surface Γ_T now corresponds to the entire new domain Ω, see figure 3.

Due to this change in the mathematical setup, the traction stresses t at the surface of the three-dimensional substrate in the 2.5D case as in (8) become part of the volume force density in the 2D case as in (12), see [17]. This leads to a displacement BVP in 2D which is easier to solve in the nonlinear case than the mixed BVP. To get a well-defined problem we need to add boundary conditions. Therefore, we assume that the substrate is larger than the support of the traction stresses, such that displacement at the boundary is negligible and we may assume zero Dirichlet boundary conditions. This assumption reflects the experimental situation well and holds, e.g. for sparsely seeded fibroblast cells that do not form connections to neighboring cells, see, e.g. figure 8, where the displacement is very small on the boundary.

Remark 3.1 (boundary conditions). Even though the Dirichlet boundary conditions are not often seen in the physical description of the model, it is an implicit assumption that often holds in TFM experiments; see figure 8(a). Indeed, many cells are placed on the same substrate and for the measurements only the displacement of some cells is measured. With a typical gel thickness of 40–50 μm and an inter-cell distance of approximately 100 μm, we can assume that neighboring cells do not interact with each other.

We can formulate the parameter-to-state-map of nonlinear TFM similarly as in the linear case as the map

$$S : X \to Y, \quad T \mapsto u \tag{13}$$

where the displacement u is the solution to the BVP (12). The Banach spaces X and Y are determined later in remark 3.8 using the existence and uniqueness results. With the specification of the forward operator S and the spaces X and Y, one can use any regularization method to solve nonlinear inverse problems. In contrast to the 2.5D case, where the operator A in (10) maps a traction stress t to a displacement u, in the 2D case the operator S maps a force density T to a displacement u. However, it is easy to convert traction stress t to force density T and vice versa by

$$T = \frac{t}{h}. \tag{14}$$

Remark 3.2 (weak form of 2D linear TFM). It is straight forward to see that if we consider Hooke's law as the constitutive equation with the linearized strain tensor, we get a linear problem with weak formulation

$$\text{find } u \in H_0^1\left(\Omega, \mathbb{R}^2\right) \quad \text{s.t.} \quad a(u, v) = \langle t, v \rangle_{L^2(\Omega, \mathbb{R}^2)} \text{ for all } v \in H_0^1\left(\Omega, \mathbb{R}^2\right) \tag{15}$$

similar to the 2.5D linear case (9), except that the force t now applies to the whole body Ω.

3.2. Well-posedness of the forward operator

To get a well-defined forward operator S, the BVP (12) needs to be solvable and the solution has to be locally unique. Unlike in the linear case in section 2, where a global unique existence result can be found easily in the literature, the problem of unique existence is more complicated in the nonlinear case.

In the following we will first show the existence of a solution via the minimization of energy in 3.2.1, then state a local uniqueness result via the Implicit Function theorem in 3.2.2 under additional regularity conditions and finally argue for a suitable choice of the Banach spaces X and Y in (13).

Similar tools have been used in [54, 68]. However, in contrast they considered elastodynamics, i.e. they obtain a time-dependent problem for the hyperelastic wave equation. In TFM the mass of the cell is too small, which is why we obtain a static problem and use the equations of elastostatics.

3.2.1. Existence of a solution via minimization of the energy. In 1976 John Ball proved the existence of a solution for general BVPs of elasticity in 1D, 2D, and 3D for nonlinear elasticity [5]. To use his results directly many conditions on the used functions must be fulfilled. He also gives a proof for the mixed BVP in 3D. Similar proofs can be found, e.g. in [16, chapter 7] or [70, section 62.13]. However we are interested in the displacement BVP in 2D. Having only Dirichlet boundary conditions is a subcase of the mixed BVP, but to get the result in 2D suitable adaptions to the proof are necessary. The main difference lies in the definition of polyconvexity and coercivity of the stored energy function, see equation (7), depending on the dimension n of the deformation gradient $F \in \mathbb{R}^{n\times n}$.

Definition 3.3 (polyconvexity). A stored energy function W is called polyconvex if there exists a convex function P such that

$$\begin{aligned} W(F) &= P(F, \det F) && \text{if } n = 2, \\ W(F) &= P(F, \operatorname{adj} F, \det F) && \text{if } n = 3. \end{aligned}$$

For $n = 3$ we need the adjugate matrix defined by $\operatorname{adj} F = \det F \cdot F^{-1}$.

Definition 3.4 (coercivity). A polyconvex stored energy function W in $\mathbb{R}^{2\times 2}$ is called coercive if

$$W(F) = P(F, \det F) \geqslant C\left(|F|_{\mathrm{F}}^{p} + |\det F|^{s}\right) + D$$

holds for the convex function P from definition 3.3 for $p \geqslant 2$, $s > 1$, $C > 0$ and $D \in \mathbb{R}$.

In the 3D case the deformation gradient F and its determinant and adjugate, $\det F$ and $\operatorname{adj} F$, describe the deformation of line, surface, and volume elements. Furthermore, in the 2D case, it holds $|\operatorname{adj} F|_{\mathrm{F}} = |F|_{\mathrm{F}}$. Therefore, in the 2D case the adjugate, $\operatorname{adj} F$, is not needed.

The next theorem ensures the existence of a solution for general polyconvex and coercive stored energy functions.

Theorem 3.5 (existence in 2D for the displacement BVP). *Let W be a polyconvex and coercive stored energy function such that*

$$\lim_{\det F \to 0} P(F, \det F) = \infty \tag{16}$$

for the convex function $P : \mathbb{M}^2 \times (0, \infty) \to \mathbb{R}$ from definition 3.3 with p and s as in definition 3.4 and the space of matrices $\mathbb{M}^2 := \{M \in \mathbb{R}^{2\times 2}\}$.

Let the force density $T \in L^p(\Omega, \mathbb{R}^2)$ and a finite reference deformation $u_0 \in V$ be given with

$$V := \left\{ u \in W^{1,p}\left(\Omega, \mathbb{R}^2\right) \mid \det(I + \nabla u) \in L^s\left(\Omega, \mathbb{R}^2\right), \det(I + \nabla u) > 0 \text{ a.e. in } \Omega \right\}. \tag{17}$$

Then for

$$G(u) = \int_\Omega W(F)\,\mathrm{d}x - \int_\Omega Tu\,\mathrm{d}x = \int_\Omega W(I + \nabla u(x))\,\mathrm{d}x - \int_\Omega Tu\,\mathrm{d}x \tag{18}$$

the problem

$$G(u) = \min!, \quad u \in U := \left\{ u \in V \middle| \; u|_{\partial\Omega} = u_0|_{\partial\Omega} \right\} \tag{19}$$

has at least one solution if $G(u_0) < \infty$.

Proof. We use the direct method to prove the theorem and follow the proof of the 3D case from [70, chapter 62.13] and [16, theorem 7.7–1] with suitable adaptions for 2D, mainly regarding coercivity and polyconvexity.

The main idea is to define a minimizing sequence of the energy G in (18). This sequence is then bounded (step ii) by the coercivity of the stored energy function and thus it converges to an element u^* (steps iii). Due to the polyconvexity, the energy is sequentially weakly lower semi-continuous which yields $G(u^*) \leqslant \inf_{u\in U} G(u)$ (step iv). The element u^* also belongs to the set U due to (16) (step v). The detailed proof can be found in appendix A. □

3.2.2. Local uniqueness of the solution via the implicit function theorem. The proof of uniqueness via the Implicit Function Theorem is based on the Banach algebra property of the spaces $W^{m,p}(\Omega, \mathbb{R}^2)$, i.e. the fact that the product of two functions of the space lies again in the space with a corresponding norm bound, which only holds true for $mp > n$, where $n = 2$ is the space dimension, see, e.g. theorem 6.1–4 from [16].

In the proof a known admissible solution in the space $W^{m,p}(\Omega, \mathbb{R}^2)$ is locally uniquely continued. We call a deformation state u admissible if the linearization of the original equation in u yields a linear strongly elliptic system with a unique solution, see [70, chapter 61.12]. Then in a small neighborhood of an admissible solution and the associated traction stress the BVP of nonlinear elasticity (12) has a unique solution.

A key ingredient to prove this statement is the Sobolev embedding $W^{1,p}(\Omega, \mathbb{R}^2) \hookrightarrow C^0(\Omega \cup \partial\Omega, \mathbb{R}^2)$ for $p > 2$, see e.g. [16, theorem 6.1–3]. Thus, in analogy to the 3D-case in [16, theorem 6.7–1], [70, theorem 61.F] or [67, chapter IV], we obtain the following result.

Theorem 3.6 (existence and uniqueness). *Let $\Omega \subset \mathbb{R}^2$ be a domain with boundary $\partial\Omega$ of class C^2 and let the stored energy function be C^∞. If we know an admissible solution $\bar{u} \in W^{2,p}(\Omega) \cap W_0^{1,p}(\Omega)$ for $p > 2$ with respective force density $\bar{T}$, then there exist neighborhoods*

$$V(\bar{u}) \in W^{2,p}(\Omega) \cap W_0^{1,p}(\Omega), \qquad W(\bar{T}) \in L^p(\Omega)$$

such that for each $T \in W$, the BVP $-\operatorname{div}(\sigma(u)) = T$ has exactly one solution $u \in V$. Moreover, the linearized operator $W^{2,p}(\Omega) \to L^p(\Omega)$, $h \mapsto -\operatorname{div}(\sigma'(u)h)$ is bounded and boundedly invertible.

It can be shown that no deformation state $u \in W^{1,p}(\Omega, \mathbb{R}^2)$ can be admissible [67, chapter 4]. Since the existence result from theorem 3.5 just gives a solution in the space $W^{1,p}(\Omega, \mathbb{R}^2)$, the regularity of this solution has to be improved to be continued uniquely as it is required in the uniqueness proof. This might be done in a similar manner as described in [42].

3.3. Finding a suitable material law

Next, we need to find a suitable material law describing the stress $\sigma(u)$. As we saw in the previous section 3.2, it is important for the existence of a solution that the stored energy function $W(F)$ of the material law be polyconvex. Unfortunately the Neo-Hookean law typically used for nonlinear TFM [48, 53, 65] is not polyconvex [61] and thus we cannot guarantee that a

solution to the respective BVP exists. For this reason, we pick a different material law from the family of polyconvex Ogden materials.

To ensure local existence and uniqueness, the stored energy function of a homogeneous, isotropic, hyperelastic (7) material should agree with the expansion

$$W(F) = \frac{\lambda}{2}(\operatorname{tr} E)^2 + \mu \operatorname{tr}\left(E^2\right) + o\left(\|E\|^2\right), \quad E = \frac{1}{2}\left(F^\top F - I\right), \tag{20}$$

with the Lamé parameters λ and μ, see (6), if it is rewritten in terms of the Green–Lagrange tensor E near a natural state, i.e. an unstressed state in which all body forces vanish. When deriving rules for the equations of elasticity, it can be shown that a constitutive equation of an isotropic, homogeneous material whose reference configuration is a natural state has to fulfill the expansion $\sigma(u) = F(\lambda(\operatorname{tr} E(u))I + 2\mu E(u) + o(E))$ near a natural state with the Green–Lagrange tensor $E(u)$ as in (3). By using the relation (7) between the constitutive equation and the stored energy function and postulating further differentiability assumptions, the expansion (20) follows. Further details and a physical intuition can be found in chapter 4.5 of [16].

Adapting theorem 4.10–2 from [16] to the two-dimensional case we get the following result.

Theorem 3.7 (Constitutive equation). *Let $\lambda, \mu > 0$ be the given Lamé constants. Then the stored energy function*

$$W(F) := \frac{\mu}{2}|F|_{\mathrm{F}}^2 + \frac{\lambda}{4}(\det F)^2 - \left(\mu + \frac{\lambda}{2}\right)\ln(\det F) - \frac{3\mu}{2} - \frac{\lambda}{4} \tag{21}$$

is polyconvex and satisfies the expansion

$$W(F) = \frac{\lambda}{2}(\operatorname{tr} E)^2 + \mu \operatorname{tr} E^2 + \mathcal{O}\left(|E|_{\mathrm{F}}^3\right). \tag{22}$$

Furthermore, it satisfies the coercivity inequality

$$W(F) \geqslant C\left(|F|_{\mathrm{F}}^2 + (\det F)^2\right) + D \tag{23}$$

for constants $C > 0$, $D \in \mathbb{R}$, if the Lamé constants fulfill the condition

$$\lambda > \frac{2\mu}{e-1}. \tag{24}$$

with Euler's number e.

Proof. We write the stored energy function (21) in the general form

$$W(F) = a|F|_{\mathrm{F}}^2 + \Gamma(\det F) + b \tag{25}$$

with a function Γ of the form $\Gamma(\delta) = c\delta^2 - d\ln\delta$ and constants $a, c, d > 0$, $b \in \mathbb{R}$. Then we determine the constants a, b, c, d such that the stored energy function W fulfills the conditions (22) and (23) as well as polyconvexity:

(i) We prove the following equations for two-dimensional matrices by simple calculations using the big $\mathcal{O}$-notation:

$$I + 2E = F^\top F$$

$$\det F^\top F = \det(I+2E) = 1+2(\operatorname{tr}E)^2 - 2\operatorname{tr}\left(E^2\right) + 2\operatorname{tr}E + \mathcal{O}\left(|E|_{\mathrm{F}}^3\right)$$
$$\Gamma(\det F) = \Gamma\left(\left(\det F^\top F\right)^{\frac{1}{2}}\right) \overset{(*)}{=} \Gamma\left(1+\operatorname{tr}E+\frac{1}{2}(\operatorname{tr}E)^2 - \operatorname{tr}E^2 + \mathcal{O}\left(|E|_{\mathrm{F}}^3\right)\right)$$
$$\overset{(**)}{=} \Gamma(1) + \Gamma'(1)\left[\operatorname{tr}E+\frac{1}{2}(\operatorname{tr}E)^2 - \operatorname{tr}E^2\right] + \frac{1}{2}\Gamma''(1)(\operatorname{tr}E)^2 + \mathcal{O}\left(|E|_{\mathrm{F}}^3\right).$$

Equality $(^*)$ holds due to the equality

$$\left(1+\operatorname{tr}E+\frac{1}{2}(\operatorname{tr}E)^2 - \operatorname{tr}E^2 + \mathcal{O}\left(|E|_{\mathrm{F}}^3\right)\right)^2 = \left(\det F^\top F\right)$$

and we get equality $(^{**})$ by applying the Taylor expansion to the function Γ. Now we simply compare the expansion (22) with the general form of the stored energy function (25). By using the derived equations for $|F|_{\mathrm{F}}^2$ and $\Gamma(\det F)$ we arrive at the system of equations

$$\begin{aligned} 3a+\Gamma(1)+b &= 0,\\ 2a+\Gamma'(1) &= 0,\\ \Gamma'(1)+\Gamma''(1) &= \lambda,\\ -\Gamma'(1) &= \mu. \end{aligned}$$

The expressions $\Gamma'(1)$ and $\Gamma''(1)$ are uniquely determined by these equations. Finally combining these equations with $\Gamma(1)=c$, $\Gamma'(1)=2c-d$, and $\Gamma''(1)=2c+d$ yields

$$a=\frac{\mu}{2},\quad c=\frac{\lambda}{4},\quad d=\mu+\frac{\lambda}{2},\quad b=-\frac{3\mu}{2}-\frac{\lambda}{4}$$

and we arrive at (25).

(ii) From the definition of the deformation gradient $F=\nabla\varphi+I$ with the deformation φ, we get the condition $\det F>0$ due to mass conservation and (25) is well-defined.

For coercivity we need an estimate of the form $cx^2 - d\ln(x) \geqslant Bx^2$, or equivalently

$$x^2 \geqslant \frac{d}{c-B}\ln(x) \tag{26}$$

for a positive constant $B>0$ and $x=\det F>0$. According to $x^2 \geqslant 2e\ln(x)$ with Euler's number e, the constant B has to fulfill $0<B\leqslant c-\frac{d}{2e}$. This is possible, i.e. $c-\frac{d}{2e}>0$, if the Lamé constants fulfill the relation

$$\lambda > \frac{2\mu}{e-1} > 1.16\mu.$$

Using equation (26) we get coercivity by

$$\begin{aligned} a|F|_{\mathrm{F}}^2 + c(\det F)^2 - d\ln(\det F) + b &\geqslant a|F|_{\mathrm{F}}^2 + B(\det F)^2 + b\\ &\geqslant \min(a,B)\left(|F|_{\mathrm{F}}^2 + (\det F)^2\right) + b. \end{aligned}$$

Since the squared norm (see, e.g. [27]) and the function $x\mapsto cx^2-d\ln(x)$ (second derivative is positive) are convex on the interval $(0,\infty)$ and the sum of convex functions is again convex, the stored energy (25) is polyconvex. □

In TFM the condition (24) for the Lamé parameters is not a problem. For a standard choice with a Poisson ratio $\nu = 0.45$ and a Young's modulus $\tilde{E} = 10\,000\,\text{Pa}$, see [53], we get Lamé constants $\lambda \approx 31\,034\,\text{Pa}$ and $\mu = 3448\,\text{Pa}$ which clearly fulfill condition (24). Now, that we have fixed a stored energy function W determining the material law, we need to compute the constitutive equation determining the stress $\sigma(u)$. The stored energy function W and the stress σ are related via $\sigma = \frac{\partial W}{\partial F}$, see (7).

Using the matrix derivation rule for the determinant $\frac{\partial \det X}{\partial X} = \det(X)X^{-\top}$, see, e.g. [45], and the chain rule on the stored energy function $W(F)$ in (21) we then get

$$\sigma(u) = \mu F + \frac{\lambda}{2}(\det F)^2 F^{-\top} - \left(\mu + \frac{\lambda}{2}\right) F^{-\top} \tag{27}$$

where we use the notation $F^{-\top} = \left(F^{-1}\right)^{\top}$.

Remark 3.8 (function space setting). The stored energy function from theorem 3.7 for $p = s > 2$ and the boundary conditions $u_0 = 0$ fulfills the conditions of theorem 3.5 for the existence of a solution and of theorem 3.6 for the uniqueness of this solution. This means that the minimization problem (19) has at least one solution $u \in W^{2,p}(\Omega, \mathbb{R}^2) \cap W_0^{1,p}(\Omega, \mathbb{R}^2)$ for a force density $T \in L^p(\Omega, \mathbb{R}^2)$. Then we can choose $X = L^p(\Omega, \mathbb{R}^2)$ and $Y = W^{2,p}(\Omega, \mathbb{R}^2) \cap W_0^{1,p}(\Omega, \mathbb{R}^2)$ in the formulation of the parameter-to-state-map (13).

We may incorporate further prior information into the space X: e.g., we may include vanishing forces on the boundary $\partial\Omega$, and higher regularity by choosing $X = H_0^1(\Omega, \mathbb{R}^2)$, equipped with the norm $\|v\|_X := \|\nabla v\|_{L^2}$ (see [37, chapter 13.2] for the norm property). By choosing the space $X = H_0^1(\Omega, \mathbb{R}^2) \hookrightarrow L^p(\Omega, \mathbb{R}^2)$ we can also remain in a Hilbert space setting.

As in the linear case in remark 2.2 the forward operator is the composition of the parameter-to-state-map and the embedding to $L^2(\Omega, \mathbb{R}^2)$. Then we get the forward operator of nonlinear 2D TFM by

$$\hat{S} : H_0^1\left(\Omega, \mathbb{R}^2\right) \hookrightarrow L^p\left(\Omega, \mathbb{R}^2\right) \to W^{2,p}\left(\Omega, \mathbb{R}^2\right) \cap W_0^{1,p}\left(\Omega, \mathbb{R}^2\right) \hookrightarrow L^2\left(\Omega, \mathbb{R}^2\right), \quad T \mapsto u.$$

The embeddings hold due to the Rellich–Kondrachov embedding theorem, see (38) in the appendix. Note that it is sufficient to consider the embedding $X = H_0^k(\Omega, \mathbb{R}^2) \hookrightarrow L^p(\Omega, \mathbb{R}^2)$ for $k \geqslant 1 - \frac{2}{p}$.

3.4. The Fréchet derivative and its adjoint

Since the operator S is nonlinear, we need to compute the Fréchet derivative of S and its adjoint, the main ingredients for solving the inverse problem with regularization algorithms as described in section 4.3.

Theorem 3.9 (Fréchet derivative). *The Fréchet derivative of the operator S that maps a given force density T to the displacement u in the function space setting from remark 3.8 is well-defined and given by $S'(T)\xi =: v$, where the function v solves*

$$\begin{cases} -\mu \operatorname{div}(\nabla v) - \left(\mu + \frac{\lambda}{2}\right) \operatorname{div}\left(F^{-\top} (\nabla v)^{\top} F^{-\top}\right) \\ -\frac{\lambda}{2} \operatorname{div}\left(2(\det F)^2 \operatorname{tr}\left(F^{-1}\nabla v\right) F^{-\top} - (\det F)^2 F^{-\top} (\nabla v)^{\top} F^{-\top}\right) = \xi \quad \text{in } \Omega \\ v = 0 \quad \text{on } \partial\Omega \end{cases} \tag{28}$$

with the deformation gradient $F = I + \nabla u$ and $u = S(T)$ solves the original problem (12).

Proof. With theorem 3.6 the Fréchet derivative exists and can be calculated using the Implicit Function Theorem. For this, we define the mapping $e : W^{2,p}(\Omega) \cap W_0^{1,p}(\Omega) \times L^p(\Omega) \to L^p(\Omega)$ by

$$e(u,T) = -\operatorname{div}(\sigma(u)) - T.$$

Then the condition $e(S(T),T) = 0$ and the Implicit Function Theorem give us that the derivative of the operator S is locally given by

$$S'(T)\xi = -\frac{\partial e}{\partial u}(S(T),T)^{-1} \circ \frac{\partial e}{\partial T}(S(T),T)\xi. \tag{29}$$

This is equivalent to the linearized problem

$$\frac{\partial e}{\partial u}(S(T),T)[S'(T)\xi] = -\frac{\partial e}{\partial T}(S(T),T)\xi.$$

Now we can compute the partial derivatives of the mapping e

$$\frac{\partial e}{\partial T}(S(T),T)\xi = -\xi, \quad \frac{\partial e}{\partial u}(S(T),T)v = \varphi'(s)|_{s=0}$$

with

$$\varphi(s) = -\operatorname{div}(\sigma(u+sv)) - T = \left(\mu + \frac{\lambda}{2}\right)\operatorname{div}\left((I+\nabla u + s\nabla v)^{-\top}\right)$$
$$-\mu\operatorname{div}(\nabla u + s\nabla v) - \frac{\lambda}{2}\operatorname{div}\left(\det(I+\nabla u+s\nabla v)^2 (I+\nabla u+s\nabla v)^{-\top}\right)$$

for $u = S(T)$. By using the chain rule and matrix differentiation rules, see e.g. [45], we arrive at

$$\varphi'(0) = -\frac{\lambda}{2}\operatorname{div}\left(2\det(F)^2 \operatorname{tr}\left(F^{-1}\nabla v\right)F^{-\top} - \det(F)^2 F^{-\top}(\nabla v)^\top F^{-\top}\right)$$
$$-\mu\operatorname{div}(\nabla v) - \left(\mu + \frac{\lambda}{2}\right)\operatorname{div}\left(F^{-\top}(\nabla v)^\top F^{-\top}\right).$$

□

Theorem 3.10. *The Fréchet derivative $S'(T)$ is self-adjoint in $L^2(\Omega)$ for all T.*

Proof. To compute the adjoint operator we use the expression for the Fréchet derivative that we get from the Implicit Function theorem (29). Then its adjoint is given by

$$(S'(T))^* g = -\left(\frac{\partial e}{\partial T}(S(T),T)\right)^* \left(\left(\frac{\partial e}{\partial u}(S(T),T)\right)^{-1}\right)^* g$$

and can be calculated via

$$(S'(T))^* g = -\left(\frac{\partial e}{\partial T}(S(T),T)\right)^* w \tag{30}$$

where the function w solves $\left(\frac{\partial e}{\partial u}(S(T),T)\right)^* w = g$. Now we compute the adjoint operator $\left(\frac{\partial e}{\partial u}(S(T),T)\right)^*$ by applying partial integration, using the boundary conditions $v, w = 0$ on $\partial\Omega$ and the equality $A : B = \operatorname{tr}(A^\top B)$. We have

$$\begin{aligned}\left\langle \frac{\partial e}{\partial u}(S(T),T)\,v,w\right\rangle_{L^2(\Omega)} &= \int_\Omega -\mu\,\mathrm{div}\,(\nabla v)\,w-\left(\mu+\frac{\lambda}{2}\right)\mathrm{div}\left(F^{-\top}(\nabla v)^\top F^{-\top}\right)w\\ &\quad-\frac{\lambda}{2}\,\mathrm{div}\left(2\,(\det F)^2\,\mathrm{tr}\left(F^{-1}\nabla v\right)F^{-\top}-(\det F)^2\,F^{-\top}(\nabla v)^\top F^{-\top}\right)w\,\mathrm{d}x\\ &= \int_\Omega\left(\mu\nabla v:\nabla w+\left(\mu+\frac{\lambda}{2}-\frac{\lambda}{2}(\det F)^2\right)\left(F^{-\top}(\nabla v)^\top F^{-\top}\right):\nabla w\right.\\ &\quad\left.+\lambda\,(\det F)^2\left(F^{-\top}:\nabla v\right)\left(F^{-\top}:\nabla w\right)\right)\mathrm{d}x\,.\end{aligned}$$

Since the trace is invariant under circular shifts, we get

$$\begin{aligned}\left(F^{-\top}(\nabla v)^\top F^{-\top}\right):\nabla w &= \mathrm{tr}\left(F^{-1}(\nabla v)\,F^{-1}(\nabla w)\right)\\ &= \mathrm{tr}\left((\nabla v)\,F^{-1}(\nabla w)\,F^{-1}\right)=\nabla v:\left(F^{-\top}(\nabla w)^\top F^{-\top}\right),\end{aligned}$$

and by a partial integration analogous to the one above we see that

$$\left\langle \frac{\partial e}{\partial u}(S(T),T)\,v,w\right\rangle_{L^2(\Omega)}=\left\langle v,\frac{\partial e}{\partial u}(S(T),T)\,w\right\rangle_{L^2(\Omega)},$$

i.e. the operator $\frac{\partial e}{\partial u}(S(T),T)$ is self-adjoint.

Since the operator $\frac{\partial e}{\partial T}(S(T),T)$ only changes the sign of its argument, i.e. $\frac{\partial e}{\partial T}(S(T),T)v=-v$, it is self-adjoint and, with equation (30), we obtain

$$S'(T)^*=-\frac{\partial e}{\partial T}(S(T),T)\left(\frac{\partial e}{\partial u}(S(T),T)\right)^{-1}=-\left(\frac{\partial e}{\partial u}(S(T),T)\right)^{-1}\frac{\partial e}{\partial T}(S(T),T)=S'(T),$$

i.e. the Fréchet derivative $S'(T)$ is self-adjoint. □

Remark 3.11 (weak form of adjoint). Since the Fréchet derivative is self-adjoint, the weak formulation of its adjoint is given by the weak formulation of (28)

$$\begin{aligned}\langle\xi,w\rangle_{L^2(\Omega)} &= \left(\mu+\frac{\lambda}{2}-\frac{\lambda}{2}(\det F)^2\right)\left\langle F^{-\top}(\nabla u)^\top F^{-\top},\nabla w\right\rangle_{L^2(\Omega)}\\ &\quad+\lambda\,(\det F)^2\,\langle\nabla u,F^{-\top}\rangle_{L^2(\Omega)}\langle\nabla w,F^{-\top}\rangle_{L^2(\Omega)}+\mu\langle\nabla u,\nabla w\rangle_{L^2(\Omega)}\end{aligned}$$

for $\xi\in L^p(\Omega,\mathbb{R}^2)$ and $u,w\in W^{2,p}(\Omega,\mathbb{R}^2)\cap W_0^{1,p}(\Omega,\mathbb{R}^2)$.

Remark 3.12. As pointed out in remark 3.8, we will consider a forward operator $\hat{S}$ defined on $H_0^1(\Omega,\mathbb{R}^2)$, equipped with the norm $\|T\|_{H_0^1}:=\|\nabla T\|_{L^2}$. Then $\hat{S}'(T)=S'(T)\circ j$ with the operator $S'(T)$ defined on $L^2(\Omega,\mathbb{R}^2)$ from theorem 3.9 and the embedding $j:H_0^1(\Omega,\mathbb{R}^2\hookrightarrow L^2(\Omega,\mathbb{R}^2)$. Then we have $\tilde{S}'[T]^*=j^*\circ S'(T)^*=j^*\circ S'(T)$. A straightforward computation shows that $j^*:L^2(\Omega,\mathbb{R}^2)\to H_0^1(\Omega,\mathbb{R}^2)$ is given by $j^*=(-\Delta)^{-1}$ with the vector Dirichlet Laplacian Δ.

4. Numerical results

In this section we test our developed methods for simulated and experimental data.

Software: For all reconstructions we use the inverse problems python library 'RegPy' [28], an in-house software specializing in regularized inversion methods. Further details can be found

on Git https://github.com/regpy/regpy. The input to RegPy is the forward operator which is either linear (8) or nonlinear (12) and its adjoint in the linear (11) or the adjoint of the derivative, see theorem 3.9, in the nonlinear case. Evaluating the forward operator means solving a BVP. To this end, we use third order finite elements on an unstructured mesh from the finite element python library NGSolve [50], a python library, alternative to FEniCS. See details on the homepage https://ngsolve.org/. The TFM codes use an existing interface between NGSolve and RegPy to implement the following numerical experiments and can be found on GROdata [49] at https://doi.org/10.25625/IBWTPH.

Data simulation: We generate the simulated noise-free data by applying the forward operators to a synthetic traction stress. To prevent committing an inverse crime, we add Gaussian noise with mean 0 and standard deviation 1 scaled by different factors and use a different FEM mesh for reconstruction. Some basic examples of inverse crimes and how to avoid them can be found in [43, chapter II]. We use Gaussian noise in accordance with the experiment, see [10, 46].

The relative noise level (in %) is calculated by

$$\text{rel. noise level} = \frac{\|\text{noise}\|_{L^2(\Omega)}}{\|\text{exact data}\|_{L^2(\Omega)}} \cdot 100. \tag{31}$$

For real data the estimation of the noise level is described in section 4.4.

Function space setting: The data space is always $Y = L^2$. In the linear case, we chose the parameter space $X = L^2$ as described in remark 2.2. For the nonlinear case we consider both $X = L^2$ and $X = H_0^1$. More details follow in section 4.3.

4.1. Simulated traction stresses

We test the reconstruction algorithms for two different force fields on a substrate with Young's modulus $\tilde{E} = 10\,\text{kPa}$ and Poisson ratio $\nu = 0.45$ which are similar to experimental data. The first force field t_1 is a symmetric ring that pulls towards the middle, see figure 4. It is defined by

$$t_1(x) = \begin{cases} a \cdot \mathrm{e}^{\frac{-1}{1-\left(x_1^2+x_2^2\right)}} \left(-x_1, -x_2, 0\right)^\top, & |x| \leqslant 1 \\ 0, & \text{else} \end{cases} \tag{32}$$

where the constant a determines the magnitude of the force. We choose $a = 1000\,\text{Pa}$. The force is embedded in a substrate of size $[-2,2]\,\mu\text{m} \times [-2,2]\,\mu\text{m}$ in both the 2.5D and 2D case. In the 2.5D case the height of the substrate is $0.6\,\mu\text{m}$.

The second force is a more realistic simplification of a cell force. It consists of four force spots embedded in a substrate of size $[-2.5,2.5]\,\mu\text{m} \times [-2.5,2.5]\,\mu\text{m}$ with height $0.6\,\mu\text{m}$ in the 2.5D case and a substrate of size $[-3,3]\,\mu\text{m} \times [-3,3]\,\mu\text{m}$ in the 2D case, see figure 5, and is defined by

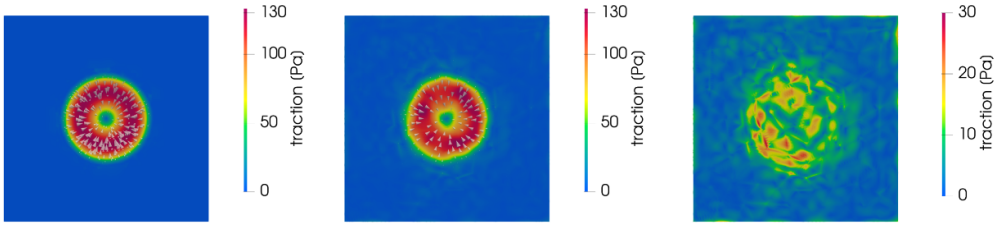

(a) Ground truth. (b) Reconstruction. (c) Error.

Figure 4. 2.5D linear TFM: simulated traction force via (32). The color code shows the magnitude of the traction stress (force per area), which is physically measured in Pa.

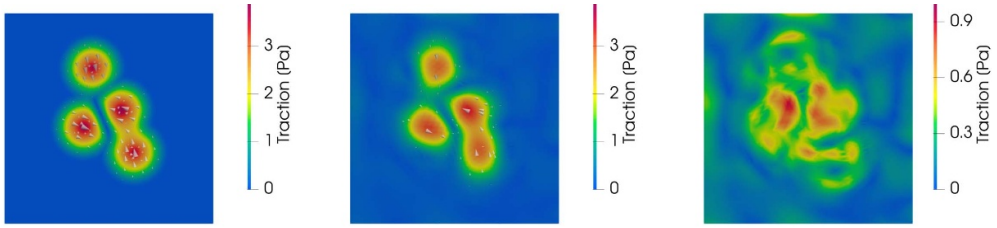

(a) Ground truth. (b) Reconstruction. (c) Error.

Figure 5. 2.5D linear TFM: simulated traction force as in (33).

$$t_2(x) = \sum_{i=1}^{4} 10\,\mathrm{Pa} \cdot \mathrm{e}^{\frac{-1}{1-|x-y^i|^2}} \left(d_1^i, d_2^i, 0\right)^\top, \quad |x-y^i| \leqslant 1, \quad \text{with}$$

i	y_1^i	y_2^i	d_1^i	d_2^i
1	−0.6	−0.2	1	−0.4
2	0.3	0.2	−1	0.4
3	0.6	−0.8	−0.2	1
4	−0.4	1.2	0.2	−1

(33)

4.2. Linear 2.5D model

Forward solver: For the forward problem we use NGSolve to find the solution of the linear BVP (8) in its weak form (9). Recall that in the 2.5D model, the traction force applies to the upper surface Γ_T. The weak solution is approximated by third order finite elements.

Inverse solver: To reconstruct the forces from noisy displacement data u^δ satisfying a noise bound $\|u - u^\delta\|_{L^2} \leqslant \delta$, we use the conjugate gradient method applied to the normal equations (CGNE). This is a fast iterative scheme which is regularized by early stopping and can be used for solving linear operator Equations in Hilbert spaces. It consists in applying the standard CG method to the normal equation

$$\hat{A}^*\hat{A}t = \hat{A}^*u^\delta \tag{34}$$

in Hilbert spaces, where the adjoint operator $\hat{A}^*$ is the solution map in the weak form (11). As a stopping criterion we use the discrepancy principle with the L^2-norm, i.e. we stop the iteration at the first iteration $k = k_{\mathrm{DP}}(\delta, u^\delta)$ for which

Table 1. Reconstruction error, noise level, run time, number of CGNE iterations and degrees of freedom of the finite element space for both forces.

	L^2-error	Noise level	Run time	Iterations	Ndof
Force field (32)	16.04%	5%	19.29 s	78	15 552
Force field (33)	29.7%	10.9%	3.77 s	9	8589

$$\|\hat{A}t_k - u^\delta\|_{L^2} \leqslant \tau\delta \tag{35}$$

holds true with a constant $\tau > 1$; in the following we choose $\tau = 1.15$. It can be shown (see [24, Thm. 3.12]) that CGNE combined with the discrepancy principle has a regularizing property, i.e. the reconstruction error $\|u_{k_{\mathrm{DP}}(\delta,u^\delta)} - u\|$ for the deterministic noise model $\|u - u^\delta\|_{L^2} \leqslant \delta$ tends to 0 as the noise level δ tends to 0. For analogous partial results with stochastic noise models we refer to [9, 31].

Reconstruction results: The reconstruction and error are displayed in figures 4 and 5. In table 1 we see that we get good reconstructions for both forces even with a higher noise level. The run time for the force field (33) is higher than for the force field (32) due to a larger finite element matrix (degrees of freedom), even though the iteration is stopped earlier resulting from a higher noise level.

4.3. Nonlinear pure 2D model

Forward solver: To numerically evaluate the nonlinear forward mapping, NGSolve solves the nonlinear minimization problem (21) by Newton's method. In particular, it finds a minimizer of the stored energy (21) using Newton's method, involving automatic differentiation for residual and tangential stiffness in each of the Newton update steps (see tutorial on elasticity https://ngsolve.org/). We observe a stable solution after 10 iterations.

Inverse solver: For solving the nonlinear inverse problem, we use the truncated Newton CG method [23, section 2]. This method, which is also available in RegPy, couples the Newton method with the Conjugate Gradient method. More precisely, after linearizing the forward operator (see theorem 3.8), the Newton equation $S'(T_k)\xi_k = u^\delta - S(T_k)$ for the update $\xi_k = T_{k+1} - T_k$ at the kth iteration (outer iteration) is solved by the CG method for its normal equation of the form $S'(T_k)^* S'(T_k)\xi_k = S'(T_k)^*\left(u^\delta - S(T_k)\right)$ (inner iteration); the adjoint $S'(T_k)^*$ is described in remark 3.11. Next, the force density is updated by $T_{k+1} = T_k + \xi_k$ (outer iteration). The inner iteration is stopped early when the residual of the inner linearized problem is reduced to a percentage $0 < \rho < 1$ of the residual of the outer nonlinear problem. We stop the outer iteration again with the discrepancy principle (35) to obtain stability. The regularizing property for this nonlinear case has been shown in [23] if the forward operator fulfills the so-called tangential cone condition and $\rho^2\tau > 2$.

Function spaces: The function space setting from remark 3.8 yields the data space $Y = L^2(\Omega, \mathbb{R}^2)$ and the parameter space $X = H_0^1(\Omega, \mathbb{R}^2)$. However, numerically we also reconstruct with $X = L^2(\Omega, \mathbb{R}^2)$, accounting for discontinuous traction. The later does not grant uniqueness (remark 3.8), but with theorem 3.5 we at least get existence. Depending on the choice of X, we use different norms when computing the solution of the normal equations in the CGNE

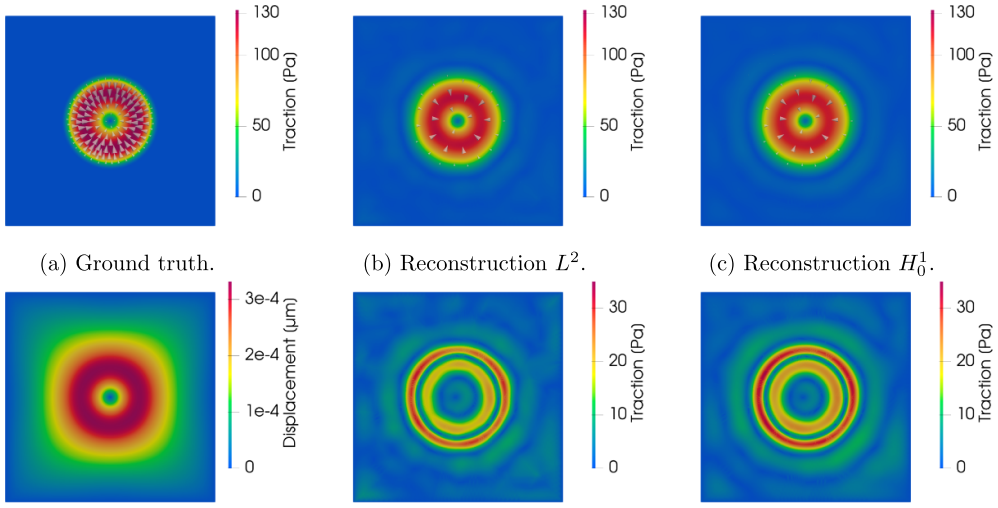

(a) Ground truth. (b) Reconstruction L^2. (c) Reconstruction H_0^1.

(d) Data. (e) Error L^2. (f) Error H_0^1.

Figure 6. 2D nonlinear TFM: simulated traction ground truth as defined in (32) (a), reconstruction with L^2-penalty (b) and H_0^1-penalty (c), noise-free displacement data (d) and error with L^2-penalty (e) and H_0^1-penalty (f).

Table 2. Reconstruction error, run time and number of Newton CG iterations of nonlinear 2D TFM for the first force (32) with a noise level of 3.64% and 2048 degrees of freedom of the finite element space. The best result is highlighted in bold.

	L^2-error	Run time	Iterations
L^2	**21.22%**	7.05 s	9
H_0^1	23.98%	22.57 s	33

method, leading to different reconstruction results. The python library RegPy [28] allows freedom in the choice of function spaces.

Reconstruction results: The parameters in the Newton-CG methods were chosen as $\rho = 0.7$ and $\tau = 1.15$. (As mentioned in [23] such a choice makes sense although not covered by the theory there.) The results for the first force field (32) are summarized in figure 6 and table 2 and for the second force field (33) in figure 7 and table 3. For both force fields we choose the effective thickness $h = 1\ \mu$m.

Even though the L^2-penalty does not incorporate the additional requirements on the traction forces t, the L^2-error is smallest for not too noisy data. However, this changes when the noise level gets larger. Then the H_0^1-penalty leads to the best result.

As described in remark 3.8 one could also perform the reconstruction in the fractional Sobolev space $X = H_0^k \subset L^p(\Omega)$ with $k \geqslant 1 - \frac{2}{p}$, where $p > 2$ suffices for uniqueness. This is in fact an interesting factor to consider and even to optimize. Work along this line includes, e.g. [29] for learning fractional order Sobolev seminorms as nonlocal regularizers in Tikhonov regularization.

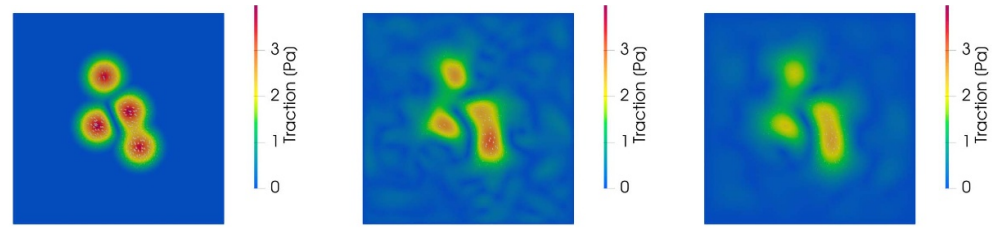

(a) Ground truth. (b) Reconstruction L^2, low noise. (c) Reconstruction H_0^1, low noise.

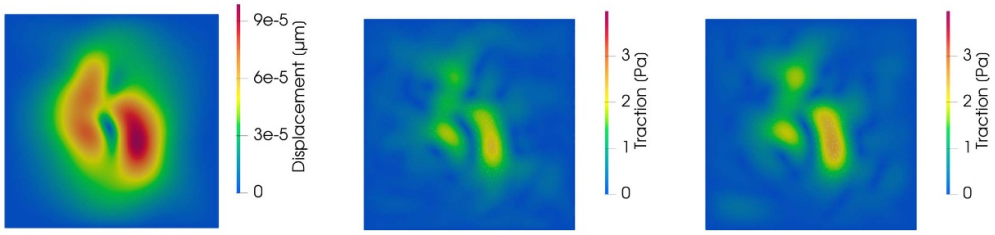

(d) Data. (e) Reconstruction L^2, high noise. (f) Reconstruction H_0^1, high noise.

Figure 7. 2D nonlinear TFM: simulated traction ground truth as in (33) (a), reconstruction with noise level of 7.81% with L^2-penalty (b) and H_0^1-penalty (c), noise-free displacement data (d) reconstruction with noise level of 15.62% with L^2-penalty (e) and H_0^1-penalty (f).

Table 3. Reconstruction error, run time and number of Newton CG iterations of nonlinear 2D TFM for the second force (33) with 5240 degrees of freedom of the finite element space. The best result is highlighted in bold.

Noise level		L^2-error	Run time	Iterations
7.81%	L^2	**51.16%**	7.65 s	6
	H_0^1	51.28%	10.04 s	7
15.63%	L^2	66.22%	4.43 s	4
	H_0^1	**57.85%**	6.48 s	5

4.4. Application to experimental data and comparison with FTTC

In the end, we apply our method to measured linear 2D displacement data from a standard TFM experiment and compare it with FTTC [10], a specific numerical realization of the popular Fourier based method introduced by physicists in [46, 47] that have shown various successful applications, as discussed in section 1.

Experimental setup: For the TFM experiment, we plate NIH 3T3 fibroblast cells on PAA gels with a Young's modulus of 34 ± 1.6 kPa and a substrate thickness of 42 μm. Fluorescently labeled carboxylated beads are added to the PAA solution as fiducial markers before it is polymerized on a treated glass bottom dish, as described in detail, e.g. in [22, 71]. After polymerization, we coat the PAA gel with Sulfo-SANPAH and fibronectin, acting as an ECM

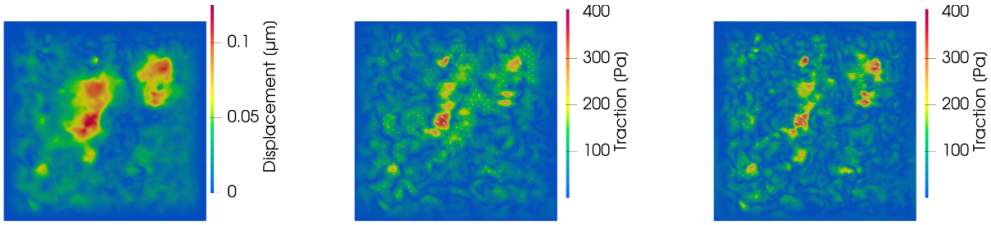

(a) Measured data. (b) Reconstruction. (c) FTTC.

Figure 8. 2D linear TFM: real data (a), our reconstruction (b), standard method (c). The field of view is of size $104.4\,\mu\text{m} \times 106\,\mu\text{m}$.

protein. TFM measurements are performed using an Olympus IX83 microscope under controlled physiological conditions. The displacements are computed using a Kanade–Lucas–Tomasi optical flow algorithm by comparing images of fiducial markers of gels with cells and of relaxed gels [12, 39]. Here, we obtain the displacement data for 72 353 points. Note that in figure 8(a) the measured displacement is very small at the boundary, justifying the homogeneous Dirichlet boundary condition in our model (13).

Preparation of data: We first collect the displacement data points from the TFM experiment. As our reconstruction procedure is formulated in a function space setting, we linearly interpolate these data points to obtain continuous data in $L^2(\Omega)$. This piecewise linear data function is then projected into the third order finite element data space. These steps are performed by NGSolve in-built functions.

To estimate the noise level, we assume that the noise is additive and homogeneous, i.e. it does not depend on the location and the functional value. Then we chose an area in the measurement data that appears to have almost no displacement and therefore lies outside the cell boundary. We compute the L^2-norm of the function on this area and scale this value to the whole domain. This results in a relative noise level of approximately 18.6%.

Reconstruction results: Since our pure 2D model, see remark 3.2, is based on the older TFM model from [17] that assumes thin substrates while the experiment is conducted under the assumptions of a not purely 2D model using thick substrates as in [18], it is not surprising that we observe differences in the reconstructions. However the results are clearly similar, see figure 8. Since our reconstructed traction has the same data range as the FTTC solution, our method also indicates that we indeed have an effective thickness $h \approx 1\,\mu$m in this experiment. Here, the discrepancy principle stops the iteration after 80 steps which needs 14.11 s.

4.5. Comparison of our linear and nonlinear 2D models

This section is dedicated to comparing linear and nonlinear models in both forward and inverse processes. All the following tests will be done in the 2D and noise-free setup, and with the traction forces described in (32).

Linear vs nonlinear forward simulation: We use the force field equation (32) with multiple values of the force strength a in the range of $[1 \times 10^2, 8 \times 10^5]$ Pa. The comparison is shown in figure 9(a), where the difference between linear and nonlinear forward simulation measured in the L^2-norm (y-axis) is only visible at large applied forces (x-axis). The difference is displayed

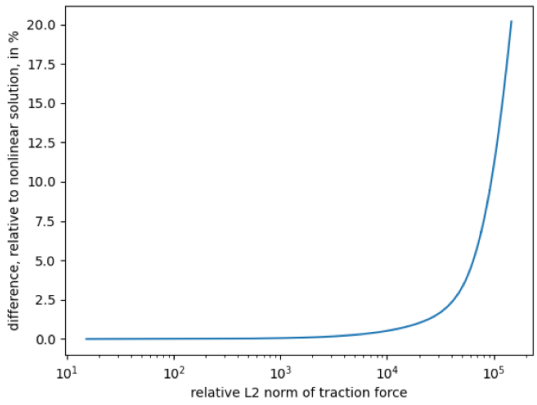

(a) Comparison of linear and nonlinear forward simulation.

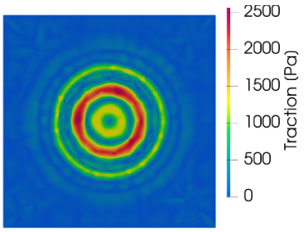

(b) Error of linear reconstruction.

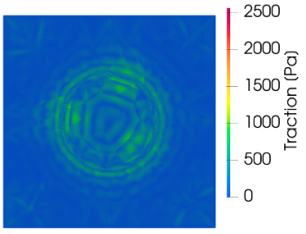

(c) Error of nonlinear reconstruction.

Figure 9. Comparison of nonlinear and linear 2D model: (a) relative difference between linear and nonlinear forward simulation (y-axis) at different source strengths (x-axis); (b) and (c) respectively show the error in the linear and nonlinear reconstruction of force field (32) with $a = 2 \cdot 10^5$ given nonlinear noise-free data.

relatively to the nonlinear displacement, and the force is displayed relative to the force that is constant one in the whole domain. This behavior motivates why mostly linear TFM is used in experiments when traction forces are sufficiently small. As an example, the relative norm of the force reconstructed with FTTC (figure 8) is 48.35, where we observe a good correlation of the results from the linear and nonlinear model. This gives an indication that it is sufficient to use the linear model in this case.

Linear vs nonlinear inversion: We now simulate the nonlinear displacement generated by the force field (32) with $a = 2 \cdot 10^5$ Pa, and use it as the input data to the linear and nonlinear inversion process. In the forward simulation process, since the force has large magnitude, its relative norm is $5.39 \cdot 10^3$, the problem becomes notably nonlinear. We thus use the incremental load method, see e.g. [11], with 10 equidistant loading steps internally in the Newton-based forward solver, in order to improve stability despite high nonlinearity. An example with explanations on the homotopy method can be found in section 3.4 of the NGSolve documentation.

Performing the reconstruction using the linear model, we get a minimal error of 7.27 after 300 CGNE iterations; see figure 9(b). Using the linear reconstruction as an initial guess to the nonlinear inversion, we can reduce the reconstruction error to 2.58% after 10 Newton CG iterations, see figure 9(c).

5. Conclusion and outlook

We described a forward model for linear 2.5D TFM and pure linear and nonlinear 2D TFM and analyzed the nonlinear parameter-to-state map S, see (13). In particular we discussed the well-definedness of the map S, showed Fréchet-differentiability and calculated its adjoint, which are essential to apply numerical regularization. Furthermore, we derived a suitable nonlinear

material law leading to a nonlinear PDE. For this setting, we established a rigorous mathematical analysis for the inverse problem of TFM from biophysics. With the nonlinear approach we developed an inverse method that can be applied to nonlinear materials with high stresses. Our approach is developed in a continuous setting, with discretization applied only at the end to preserve the mathematical properties of the involved functions, particularly the solution, as long as possible. Furthermore, our analysis and the inclusion in the Python toolbox RegPy [28] allow to easily use different regularization algorithms instead of using standard Tikhonov regularization as commonly used in the physics community in TFM. In the linear 2D case, where we applied our methods to experimental data, we observe a good agreement of our results and the ones obtained from the FTTC method. In the nonlinear 2D case and the linear 2.5D case, we obtained conclusive results for synthetic data and were able to reduce artifacts by incorporating the nature of the traction forces.

An advantage of the proposed approach is its flexibility allowing for a number of extensions and variations. For example, we could work with other specific nonlinear material laws. For these experimentally new settings our findings may serve as a fundamental mathematical approach. Additionally, other *a-priori* information as, e.g. known support of the traction stress, the equilibrium condition, symmetry assumptions, or sparsity with respect to certain frames, could be incorporated into the optimization problem. Furthermore, the mathematical analysis and implementation of TFM could be extended to 3D TFM.

Data availability statement

The code and data that support the findings of this article are openly available on GROdata [49] at https://doi.org/10.25625/IBWTPH.

Acknowledgments

The authors thank E Klass for help with the implementation. G Sarnighausen, T Nguyen, A Wald, T Hohage and S Köster acknowledge funding by Deutsche Forschungsgemeinschaft (DFG, German Research Foundation)—CRC 1456 (Project-ID 432680300), Projects A04, B06 and C03. A Wald, S Köster and T Betz additionally acknowledge support by DFG RTG 2756 (Project-ID 449750155), Projects A2, A4, A7, B3, and S Köster and T Betz acknowledge support in the framework of Germany's Excellence Strategy, EXC 2067/1 (Project-ID 390729940). S Köster, T Betz and U S Schwarz are members of the Max Planck School Matter to Life supported by the German Federal Ministry of Education and Research (BMBF) in collaboration with the Max Planck Society.

Appendix. Proof of lemma 3.5

We use $\lesssim$, $\gtrsim$ and $\simeq$ for relations up to multiplicative constants independent of u and v.

(i) Preliminaries. To ensure the positivity constraint we define

$$\bar{P}(F,\det F) = \begin{cases} P(F,\det F) & \text{if } \det F > 0 \\ +\infty & \text{if } \det F \leqslant 0 \end{cases}$$

with the function P as in definition 3.4. The convex function P is continuous according to proposition 47.5 in [70]. Therefore, the function $\bar{P} : \mathbb{M}^2 \times (0,\infty) \to (-\infty,\infty]$ is

continuous because of (16). Furthermore, we set

$$X := W^{1,p}(\Omega,\mathbb{R}^2) \times L^s(\Omega,\mathbb{R}^2)$$
$$Hu(x) := \big(x+u(x), \det(I+\nabla u(x)\big) \in X$$

for $u \in W^{1,p}(\Omega,\mathbb{R}^2)$.

(a) On the space $W^{1,p}(\Omega,\mathbb{R}^2)$ we introduce the norm

$$\|v\|_{1,p} := \left(\int_\Omega |\nabla v|_{\mathrm{F}}^p \,\mathrm{d}x + \int_{\partial\Omega} |v|_{\mathrm{F}}^p \,\mathrm{d}s\right)^{\frac{1}{p}},$$

which is equivalent to the standard norm on the space $W^{1,p}(\Omega,\mathbb{R}^2)$, see e.g. [55, § 114, theorem 3]. Then, for all elements $v(x) = x + u(x)$ with $u \in U$, we have

$$\|v\|_{1,p}^p \lesssim \|\nabla v\|_{L^p(\Omega,\mathbb{R}^2)}^p + C_{u_0} \qquad \text{with} \qquad C_{u_0} := \|x+u_0\|_{L^p(\partial\Omega,\mathbb{R}^2)}^p \tag{36}$$

since for $u \in U$ holds $u = u_0$ on the boundary $\partial\Omega$ and thus the boundary integral has the same value for all elements $u \in U$. On the space X we choose the norm $\|v\|_X := \|v_1\|_{1,p} + \|v_2\|_s$ for $v = (v_1, v_2) \in \mathbb{X}$.

(b) Theorem of Mazur. Let the sequence (v_n) in an arbitrary Banach space Y converge weakly to some element $v \in Y$, i.e. $v_n \rightharpoonup v$ in Y as $n \to \infty$. Then there exist convex linear combinations $w_n = \sum_{i=1}^{N(n)} \lambda_{ni} v_i$ with $\sum_{i=1}^{N(n)} \lambda_{ni} = 1$, $\lambda_{ni} > 0$ such that $N(n) \to \infty$ as $n \to \infty$, and we have strong convergence $w_n \to v$ in the space Y as $n \to \infty$, see, e.g. [14, Lemma 3.1.20].

(c) Recall that in case of convergence $f_n \to f$ in $L^p(\Omega)$ as $n \to \infty$ and $1 \leqslant p \leqslant \infty$, there exists a subsequence—for simplicity also called f_n—such that the subsequence converges almost everywhere, i.e. $f_n(x) \to f(x)$ a.e. in Ω as $n \to \infty$, according to the Riesz–Fischer theorem [20, chapter VI, section 2].

(ii) Minimal sequence. Define the infimum $m := \inf_{u\in U} G(u)$. We show that there exists an element $u^* \in U$ with $G(u^*) = m$. Due to the coercivity we have $-\infty < G(u) \leqslant \infty$ for all elements $u \in U$. Since $G(u_0) < \infty$, the infimum m is finite.

We choose a sequence (u_n) in the space U such that $G(u_1) \geqslant G(u_2) \geqslant \ldots \geqslant G(u_n) \to m$ as $n \to \infty$ and show that the sequence (Hu_n) is bounded in X. Using (36) and definition 3.4 we obtain

$$\begin{aligned}
\tilde{H}(u_n) &:= \|x+u_n(x)\|_{1,p}^p + \|\det(I+\nabla u_n)\|_{L^s(\Omega,\mathbb{R}^2)}^s \\
&\overset{(36)}{\lesssim} \|I+\nabla u_n(x))\|_{L^p(\Omega,\mathbb{R}^2)}^p + \|\det(I+\nabla u_n)\|_{L^s(\Omega,\mathbb{R}^2)}^s + C_{u_0} \\
&\simeq \|I+\nabla u_n(x))\|_{L^p(\Omega,\mathbb{R}^2)}^p + \|\det(I+\nabla u_n)\|_{L^s(\Omega,\mathbb{R}^2)}^s + C_{u_0} - \frac{1}{p}\|I+\nabla u_n(x))\|_{L^p(\Omega,\mathbb{R}^2)}^p \\
&\overset{3.4}{\lesssim} \int_\Omega P(I+\nabla u_n, \det(I+\nabla u_n)\,\mathrm{d}x - \frac{1}{p}\|I+\nabla u_n(x))\|_{L^p(\Omega,\mathbb{R}^2)}^p + C_{u_0} - D.
\end{aligned}$$

To get rid of the power p we use the Bernoulli inequality which states $(1+x)^p \geqslant 1+px$ for $x \geqslant -1$ and $p \geqslant 1$. With the substitution $a = 1+x$ it follows $-\frac{a^p}{p} \leqslant -a - C_p$ for $a \geqslant 0$ with $C_p := (1-p)/p$. Thus

$$\tilde{H}(u_n) \lesssim \int_\Omega P(I+\nabla u_n, \det(I+\nabla u_n)\,\mathrm{d}x - \|I+\nabla u_n(x)\|_{L^p(\Omega,\mathbb{R}^2)} - C_p + C_{u_0} - D.$$

To relate $\|I+\nabla u_n(x)\|_{L^p(\Omega,\mathbb{R}^2)}$ and $\|u_n(x)\|_{1,p}$ we observe

$$\begin{aligned}\|u_n(x)\|_{1,p} &= \|I+\nabla u_n(x) - I\|_{L^p(\Omega,\mathbb{R}^2)} + \|u_0\|_{L^p(\partial\Omega,\mathbb{R}^2)} \\ &\leqslant \|I+\nabla u_n(x)\|_{L^p(\Omega,\mathbb{R}^2)} + \|u_0\|_{L^p(\partial\Omega,\mathbb{R}^2)} + \|I\|_{L^p(\Omega,\mathbb{R}^2)}\end{aligned} \tag{37}$$

and with $C_{u_0'} := \|u_0\|_{L^p(\partial\Omega,\mathbb{R}^2)} + \|I\|_{L^p(\Omega,\mathbb{R}^2)}$ we get

$$\tilde{H}(u_n) \overset{(A2)}{\lesssim} \int_\Omega P(I+\nabla u_n, \det(I+\nabla u_n)\,\mathrm{d}x - \|u_n(x)\|_{1,p} + C_{u_0'} - C_p + C_{u_0} - D.$$

Next we estimate the $W^{1,p}$-norm by the $L^{\frac{p}{p-1}}$-norm. The embedding $W^{1,p}(\Omega,\mathbb{R}^2) \hookrightarrow L^{\frac{p}{p-1}}(\Omega,\mathbb{R}^2)$ is compact and thus continuous due to the Rellich–Kondrachov theorem

$$W^{k_1,p_1}\left(\Omega,\mathbb{R}^2\right) \hookrightarrow W^{k_2,p_2}\left(\Omega,\mathbb{R}^2\right), \quad \text{if } \frac{k_1-k_2}{2} > \frac{1}{p_1} - \frac{1}{p_2}, k_1 \geqslant k_2, \tag{38}$$

for $k_1,k_2 \in \mathbb{N}_0, p_1,p_2 \geqslant 1$, see, e.g. [1, chapter 6], which is fulfilled for $k_1 = 1$, $k_2 = 0$, $p_1 = p$ and $p_2 = \frac{p}{p-1}$ because $p \geqslant 2$. Finally we get

$$\begin{aligned}\tilde{H}(u_n) &\overset{(A3)}{\lesssim} \int_\Omega W(I+\nabla u_n)\,\mathrm{d}x - \|T\|_{L^p(\Omega,\mathbb{R}^2)}\|u_n(x)\|_{L^{\frac{p}{p-1}}(\Omega,\mathbb{R}^2)} + C_{u_0'} - C_p + C_{u_0} - D \\ &\lesssim \int_\Omega W(I+\nabla u_n)\,\mathrm{d}x - \int_\Omega Tu_n\,\mathrm{d}x + C_{u_0'} - C_p + C_{u_0} - D \\ &= G(u_n) + C_{u_0'} - C_p + C_{u_0} - D\end{aligned}$$

This is bounded because all the constants are bounded and $G(u_n) \leqslant G(u_1)$ for all $n \in \mathbb{N}$. Now since $\|x+u_n(x)\|_{1,p}^p + \|\det(I+\nabla u_n)\|_{L^s(\Omega,\mathbb{R}^2)}^s$ is bounded, the expression without powers $\|Hu_n\|_X$ is bounded as well.

(iii) Weak and strong convergence. Since the space X is reflexive, there exists a subsequence, denoted again by (Hu_n) that converges weakly to an element $v \in X$, i.e. $Hu_n \rightharpoonup v$ in X as $n \to \infty$. Theorem 6.2 in [5] implies $v = Hu^*$ for an element $u^* \in U$.
For each element $v_n = Hu_n$, there exists a convex linear combination w_n of Hu_i from Mazur's theorem as in (i)b). By possibly passing to a subsequence, it holds $w_n \to Hu^*$ in X and $w_n(x) \to Hu^*(x)$ a.e. in Ω as $n \to \infty$.

(iv) Lemma of Fatou. The convexity of the function P yields $P(w_n) \leqslant \sum_{i=1}^{N(n)} \lambda_{ni} P(Hu_i)$. From the coercivity condition follows $P(w_n) \geqslant D$ for all n with the constant D from (3.4), and the Lemma of Fatou (see e.g. [70, appendix]) and pointwise convergence of the convex linear combinations w_n from (iii) yield

$$\int_\Omega \bar{P}(u^*)\,\mathrm{d}x = \int_\Omega \lim_{n\to\infty} P(w_n)\,\mathrm{d}x \leqslant \lim_{n\to\infty} \int_\Omega \sum_{i=1}^{N(n)} \lambda_{ni} P(Hu_i)\,\mathrm{d}x.$$

We define $\bar{G}$ by $\bar{G}(u) = \int_\Omega P(F,\det F) - Tu\,\mathrm{d}x$. Then we get

$$\bar{G}(u^*) = \int_\Omega \bar{P}(u^*)\,\mathrm{d}x - \int_\Omega Tu^*\,\mathrm{d}x \leqslant \lim_{n\to\infty} \sum_{i=1}^{N(n)} \lambda_{ni} G(u_i) \overset{(1)}{=} \lim_{n\to\infty} G\left(u_{N(n)}\right) = m \tag{39}$$

where equality (1) holds because the expressions $G(u_{N(n)})$ and $\sum_{i=1}^{N(n)} \lambda_{ni} G(u_i)$ have the same limit due to the condition $\sum_{i=1}^{N(n)} \lambda_{ni} = 1$, $\lambda_{ni} > 0$. So the limit point u^* is a minimizer of the energy G.

(v) It remains to show that the minimizer u^* is an element of the space U. Due to the condition $\bar{P}(u^*) < \infty$, the construction of the function $\bar{P}$ yields $\det(I + \nabla u^*(x)) > 0$ a.e. in Ω. Since $u_n = u_0$ on the boundary $\partial\Omega$ for all n, and since convex linear combinations of the elements u_n converge to the minimizer $u^* \in W^{1,p}(\Omega, \mathbb{R}^2)$, we also have $u^* = u_0$ on the boundary $\partial\Omega$. Thus (39) is equivalent to $G(u^*) = m$ and $u^* \in U$.

ORCID iDs

Gesa Sarnighausen https://orcid.org/0009-0003-2677-6499
Tram Thi Ngoc Nguyen https://orcid.org/0000-0002-7245-7611
Thorsten Hohage https://orcid.org/0000-0002-5408-2780
Mangalika Sinha https://orcid.org/0009-0005-3709-819X
Sarah Köster https://orcid.org/0000-0002-0009-1024
Timo Betz https://orcid.org/0000-0002-1548-0655
Ulrich Sebastian Schwarz https://orcid.org/0000-0003-1483-640X
Anne Wald https://orcid.org/0000-0001-6149-8576

References

[1] Adams R A and Fournier J J F 2003 *Sobolev Spaces* (Elsevier Science)
[2] Ahmed W W, Fodor E and Betz T 2015 Active cell mechanics: measurement and theory *Biochim. Biophys. Acta, Mol. Cell Res.* **1853** 3083–94
[3] Ambrosi D 2006 Cellular traction as an inverse problem *SIAM J. Appl. Math.* **66** 2049–60
[4] Ambrosi D, Duperray A, Peschetola V and Verdier C 2009 Traction patterns of tumor cells *J. Math. Biol.* **58** 163–81
[5] Ball J 1976 Convexity conditions and existence theorems in nonlinear elasticity *Arch. Ration. Mech. Anal.* **63** 337–403
[6] Banerjee S, Gardel M and Schwarz U S 2020 The actin cytoskeleton as an active adaptive material *Annu. Rev. Condens. Matter Phys.* **11** 421–39
[7] Bar-Kochba E, Toyjanova J, Andrews E, Kim K-S and Franck C 2014 A fast iterative digital volume correlation algorithm for large deformations *Exp. Mech.* **55** 261–74
[8] Barrasa-Fano J, Shapeti A, De Jong J, Ranga A, Sanz-Herrera J and Van Oosterwyck H 2021 Advanced in silico validation framework for three-dimensional traction force microscopy and application to an in vitro model of sprouting angiogenesis *Acta Biomater.* **126** 326–38
[9] Blanchard G and Mathé P 2012 Discrepancy principle for statistical inverse problems with application to conjugate gradient iteration *Inverse Problems* **28** 115011
[10] Blumberg J and Schwarz U S 2022 Comparison of direct and inverse methods for 2.5D traction force microscopy *PLoS One* **17** 1–25, 01
[11] Botti L and Verzeroli L 2022 BR2 discontinuous Galerkin methods for finite hyperelastic deformations *J. Comput. Phys.* **463** 111303
[12] Bouguet J-Y 1999 Pyramidal implementation of the lucas kanade feature tracker
[13] Bower A F 2009 *Applied Mechanics of Solids* (Taylor & Francis)
[14] Bühler T and Salamon D 2018 Functional Analysis (*Graduate Studies in Mathematics* 191)
[15] Butler J, Tolić-Nørrelykke I, Fabry B and Fredberg J 2002 Traction fields, moments and strain energy that cells exert on their surroundings *Am. J. Phys. Cell Phys.* **282** C595–605
[16] Ciarlet P G 1994 *Three-Dimensional Elasticity Number Bd. 20 in Mathematical Elasticity* (Elsevier Science)
[17] Dembo M, Oliver T, Ishihara A and Jacobson K 1996 Imaging the traction stresses exerted by locomoting cells with the elastic substratum method *Biophys. J.* **70** 2008–22

[18] Dembo M and Wang Y-L 1999 Stresses at the cell-to-substrate interface during locomotion of fibroblasts *Biophys. J.* **76** 2307–16
[19] Denisin A, Kim H, Riedel-Kruse I and Pruitt B 2024 Field guide to traction force microscopy *Cell. Mol. Bioeng.* **17** 04
[20] Elstrodt J 2018 *Maß- und Integrationstheorie* 8 edn (Springer)
[21] Franck C, Hong S, Maskarinec S, Tirrell D and Ravichandran G 2007 Three-dimensional full-field measurements of large deformations in soft materials using confocal microscopy and digital volume correlation *Exp. Mech.* **47** 427–38
[22] Hanke J, Probst D, Zemel A, Schwarz U S and Köster S 2018 Dynamics of force generation by spreading platelets *Soft Matter* **14** 6571–81
[23] Hanke M 1997 Regularizing properties of a truncated Newton-CG algorithm for nonlinear inverse problems *Numer. Funct. Anal. Optim.* **18** 971–93
[24] Hanke M 1995 *Conjugate Gradient Type Methods for Ill-Posed Problems* (Chapman and Hall/CRC)
[25] Harris A K, Stopak D and Wild P 1981 Fibroblast traction as a mechanism for collagen morphogenesis *Nature* **290** 249–51
[26] Harris A K, Wild P and Stopak D 1980 Silicone rubber substrata: a new wrinkle in the study of cell locomotion *Science* **208** 177–9
[27] Hartmann S and Neff P 2003 Polyconvexity of generalized polynomial-type hyperelastic strain energy functions for near-incompressibility *Int. J. Solids Struct.* **40** 2767–91
[28] Hohage T, Mickan P, Müller B, Oberender F, and Rügge C 2024 regpy: python tools for regularization methods
[29] Holler G and Kunisch K 2022 Learning nonlocal regularization operators *AIMS* **12** 81–114
[30] Holzapfel G A 2000 *Nonlinear Solid Mechanics: A Continuum Approach for Engineering* (Wiley)
[31] Hucker L and Reiß M 2024 Early stopping for conjugate gradients in statistical inverse problems (arXiv:2406.15001)
[32] Hur S *et al* 2012 Roles of cell confluency and fluid shear in 3-dimensional intracellular forces in endothelial cells *Proc. Natl Acad. Sci.* **109** 11110–5
[33] Hur S, Zhao Y, Li Y -S, Botvinick E and Chien S 2009 Live cells exert 3-dimensional traction forces on their substrata *Cell. Mol. Bioeng.* **2** 425–36
[34] Kristal-Muscal R, Dvir L and Weihs D 2013 Metastatic cancer cells tenaciously indent impenetrable, soft substrates *New J. Phys.* **15** 035022
[35] Landau L D, Pitaevskii L P, Kosevich A M and Lifshitz E M 1986 Theory of Elasticity: Volume 7 *Course of Theoretical Physics* (Elsevier Science)
[36] Lekka M, Gnanachandran K, Kubiak A, Zieliński T and Zemła J 2021 Traction force microscopy - measuring the forces exerted by cells *Micron* **150** 103138
[37] Leoni G 2009 *A First Course in Sobolev Spaces* 2 edn (*Graduate studies in mathematics* Vol 181) (American Mathematical Society)
[38] Lorenz C and Köster S 2022 Multiscale architecture: mechanics of composite cytoskeletal networks *Biophys. Rev.* **3** 031304
[39] Lucas B D and Kanade T 1981 An iterative image registration technique with an application to stereo vision *Int. Joint Conf. on Artificial Intelligence*
[40] Maskarinec S, Franck C, Tirrell D and Ravichandran G 2009 Quantifying cellular traction forces in three dimensions *Proc. Natl Acad. Sci.* **106** 22108–13
[41] Michel R, Peschetola V, Vitale G, Etienne J, Duperray A, Ambrosi D, Preziosi L and Verdier C 2013 Mathematical framework for traction force microscopy *ESAIM Proc.* vol 42 p 12
[42] Morrey C B 1966 *Regularity Theorems for the Solutions of General Elliptic Systems and Boundary Value Problems* (Springer) pp 209–86
[43] Mueller J L and Siltanen S 2012 *Linear and Nonlinear Inverse Problems with Practical Applications* (Society for Industrial and Applied Mathematics)
[44] Ng M R, Besser A, Brugge J S and Danuser G 2014 Mapping the dynamics of force transduction at cell-cell junctions of epithelial clusters *eLife* **3** e03282
[45] Petersen K B and Pedersen M S 2012 *The Matrix Cookbook* (Technical University of Denmark)
[46] Plotnikov S V, Sabass B, Schwarz U S and Waterman C M 2014 High-Resolution Traction Force Microscopy *Quantitative Imaging in Cell Biology* (*Methods in Cell Biology*) vol 123, ed C W Jennifer and T Wittman (Academic) ch 20, pp 367–94
[47] Sabass B, Gardel M L, Waterman C M and Schwarz U S 2008 High resolution traction force microscopy based on experimental and computational advances *Biophys. J.* **94** 207–20

[48] Sanz-Herrera J A, Barrasa-Fano J, Cóndor M and Van Oosterwyck H 2021 Inverse method based on 3D nonlinear physically constrained minimisation in the framework of traction force microscopy *Soft Matter* **17** 10210–22
[49] Sarnighausen G *et al* 2025 Data for 'Traction force microscopy for linear and nonlinear elastic materials as a parameter identification inverse problem.' *GRO.data* (https://doi.org/10.25625/IBWTPH)
[50] Schöberl J 2014 *ASC Reports* ASC Report 30/2014 Institute of Analysis and Scientific Computing pp 1–23
[51] Schwarz U S 2017 Mechanobiology by the numbers: a close relationship between biology and physics *Nat. Rev. Mol. Cell Biol.* **18** 711–2
[52] Schwarz U S, Balaban N Q, Riveline D, Bershadsky A, Geiger B and Safran S A 2002 Calculation of forces at focal adhesions from elastic substrate data: the effect of localized force and the need for regularization *Biophys. J.* **83** 1380–94
[53] Schwarz U S and Soiné J 2015 Traction force microscopy on soft elastic substrates: a guide to recent computational advances *Biochimica et Biophysica Acta* **1853** 3095–104
[54] Seydel J and Schuster T 2016 On the linearization of identifying the stored energy function of a hyperelastic material from full knowledge of the displacement field *Math. Methods Appl. Sci.* **40** 183–204
[55] Smirnov V I 1964 Metric and normed spaces *A Course of Higher Mathematics* (*International Series of Monographs on Pure and Applied Mathematics*) vol 62, ed V I Smirnov (Pergamon) ch 4, pp 257–366
[56] Soiné J 2014 Reconstruction and simulation of cellular traction forces *PhD Thesis* Heidelberg University
[57] Soiné J, Brand C, Stricker J, Oakes P, Gardel M and Schwarz U S 2015 Model-based traction force microscopy reveals differential tension in cellular actin bundles *PLoS Comput. Biol.* **11** e1004076
[58] Steinwachs J, Metzner C, Skodzek K, Lang N, Thievessen I, Mark C, Münster S, Aifantis K E and Fabry B 2016 Three-dimensional force microscopy of cells in biopolymer networks *Nat. Methods* **13** 171–6
[59] Stout D A, Bar-Kochba E, Estrada J B, Toyjanova J, Kesari H, Reichner J S and Franck C 2016 Mean deformation metrics for quantifying 3d cell-matrix interactions without requiring information about matrix material properties *Proc. Natl Acad. Sci.* **113** 201510935
[60] Style R, Boltyanskiy R, German G, Hyland C, MacMinn C, Mertz A, Wilen L, Xu E and Dufresne E R 2014 Traction force microscopy in physics and biology *Soft Matter* **10** 04
[61] Suchocki C and Jemioło S 2021 Polyconvex hyperelastic modeling of rubberlike materials *J. Braz. Soc. Mech. Sci. Eng.* **43** 352
[62] Tambe D, Croutelle U, Trepat X, Park C, Kim J H, Millet E, Butler J and Fredberg J 2013 Monolayer stress microscopy: limitations, artifacts and accuracy of recovered intercellular stresses *PLoS One* **8** e55172
[63] Tambe D T *et al* 2011 Collective cell guidance by cooperative intercellular forces *Nature Materials* **10** 469–75
[64] Tartar L 2007 *The Equivalence Lemma; Compact Embeddings* (Springer) pp 53–57
[65] Toyjanova J, Bar-Kochba E, López-Fagundo C, Reichner J, Hoffman-Kim D and Franck C 2014 High resolution, large deformation 3D traction force microscopy *PLoS One* **9** 1–12
[66] Toyjanova J, Hannen E, Bar-Kochba E, Darling E, Henann D and Franck C 2014 3D viscoelastic traction force microscopy *Soft Matter* **10** 08
[67] Valent T 1988 *Boundary Value Problems of Finite Elasticity: Local Theorems on Existence, Uniqueness and Analytic Dependence on Data* (Springer Tracts in Natural Philosophy Springer)
[68] Wöstehoff A and Schuster T 2015 Uniqueness and stability result for cauchy's equation of motion for a certain class of hyperelastic materials *Appl. Anal.* **94** 1561–93
[69] Zancla A, Mozetic P, Orsini M, Forte G and Rainer A 2022 A primer to traction force microscopy *J. Biological Chem.* **298** 101867
[70] Zeidler E H 1997 *Nonlinear Functional Analysis and its Applications: IV: Applications to Mathematical Physics* (Springer)
[71] Zelená A, Blumberg J, Probst D, Gerasimaitė R, Lukinavičius G, Schwarz U S and Köster S 2023 Force generation in human blood platelets by filamentous actomyosin structures *Biophys. J.* **122** 3340–53